UNIVERSITÀ DEGLI STUDI DI PADOVA

PHASOR APPROACH

TO FLUORESCENCE LIFETIME MICROSCOPY

TO MEASURE

STEM CELL DIFFERENTIATION

Corso di Laurea Magistrale in

Bioingegneria

Laureanda:
Ottavia Golfetto

Relatore:
Chiar.mo Prof. Alfredo Ruggeri

Correlatore:
Chiar.mo Prof. Enrico Gratton

Anno Accademico 2009-2010

A mia madre e a mio nonno.
Le mie guide,
da sempre e per sempre.

Contents

The Fascination of Stem Cells

Pluripotent stem cells have two impressive properties: immortality and pluripotency. The first property, the immortality, gives them the capacity of indefinite self-renewal. The second property, the pluripotency, makes them able to give rise to all the tissues of the adult body [1].

The first time I heard about stem cells, they reminded me a concept which was developed in Art and Philosophy, during the Romanticism period but had already the basis in Latin Literature: the concept of the "Sublime". The "Sublime" is the quality of greatness or vast magnitude, whether physical, intellectual, metaphysical or artistic. The concept especially refers to a greatness with which nothing else can be compared and which is beyond all possibility of calculation, measurement or imitation. The men are fascinated and attracted by objects which express the sense of sublime because they can see this enormous potential but they cannot comprehend it throughly.

Pluripotent stem cells represents worthily this kind of sensation. We can see the big potentiality they have, but many of their features are still unknown.

Pluripotent stem cells have been derived from the human embryo (human embryonic stem cells hES) [2][3] and induced pluripotent stem cells (iPS) have been developed through the reprogramming of adult human cells [4][5]. hES and iPS keep in themselves the promise of revolutionizing biomedical research. Investigations into how pluripotency is maintained and about the mechanism of lineage commitment, are important not only to understand cellular differentiation but especially to develop stem-cell-based therapies for regenerative medicine. Stem cell plasticity might enable the body to compensate for cellular loss and to respond to the demands for cell production during tissue maintenance, remodelling, regeneration and repair.

One crucial point with respect to stem cells is understanding their division, which can be symmetric or asymmetric. Pluripotent stem cells are self-renewing. This means that they are able to product exclusively daughter cells which maintain stem-cell identity, or they can divide both into undifferentiated daughters and daughters which start differentiating in specialized

tissues. The first type of division is called symmetric while the second one is called asymmetric. Many studies are investigating the possible extrinsic and intrinsic signaling involved in the two different divisions [1]. Especially, we are interested in understanding when the specific division is decided, and the possible answers to this question would influence the directions of the research. If the cell fate is already decided by intrinsic transcription factors, the direction of research would be discriminating the different cell fates in order to choose the appropriate cells for different applications. If the cell fate is only conditioned by extrinsic signaling, the direction would be understanding which external factors can induce the stem cells to follow the desired pathway.

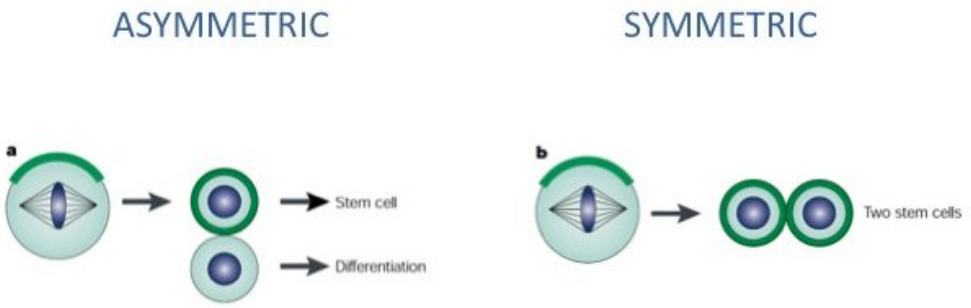

Figure (1). *Representation of asymmetric and symmetric division. Asymmetric division products both undifferentiated stem cells and cells which start differentiation. Symmetric division generates only undifferentiated stem cells.*

Recently, several transcription factors showed to be extremely useful to identify the stage of stem cell differentiation in vitro. Among them, Oct4, Nanog and Sox2 are the most common [1]. These transcription factors are highly expressed by pluripotent stem cells and when stem cells start differentiating their expression becomes lower and lower. However, transcription factors can show the stage of differentiation but they are not able to give information about cellular signaling. Besides, their visualization require strongly invasive procedures which can be performed only in vitro.

Following these lines of thought, the project I followed for this thesis work was conceived. We wanted to investigate stem cells differentiation not only to measure the stage of differentiation, but also to try to comprehend a little bit more about factors and chemical changes involved in stem cells division. Furthermore, the optical method we developed has the potential of being non invasive and of allowing dynamic investigation in vivo.

Substantially, this thesis work has been an attempt to decrease, even just a little bit, the sense of "Sublime" and mysterious which stem cells inspire.

Summary

In this thesis work, we developed a label-free imaging method to monitor stem cells in vivo. We performed the following steps.

We used intrinsic fluorescence biomarkers of biological samples and we acquired Fluorescence Lifetime Microscopy (FLIM) images of undifferentiated and differentiating stem cells . We used the phasor approach to analyze the acquired FLIM images [6]. The phasor approach is an innovative approach which differs completely from the usual approach of multiexponential fitting of lifetimes decay. It allows a straightforward interpretation of intrinsic fluorescence signal in living tissues directly in terms of physiological relevant fluorophores, without the calculation of fluorescence lifetimes. The phasor approach offers a label-free imaging method to monitor stem cells in vivo and to measure their stage of differentiation.

Understanding of physiological processes in tissues usually requires complex and invasive labeling procedures, such as Immunostaining of Oct4. This standard and currently used procedure requires the fixation and the extrinsically labeling of the cells through antibodies and Alexa Fluor 568.

The method we developed is label-free and completely non invasive. We used our method to locate intrinsic fluorophores, such as collagen, retinol, retinoic acid, flavins, nicotinamide adenine nucleotide (NADH) and porphyrin by their phasor signature. We provided images of fluorescent species based on their decay properties rather than resolving the lifetime of molecular species. We separated multiple intrinsic fluorophores by cluster analysis of the phasor distribution in FLIM images of human embryonic stem cells (hES). We used intrinsic fluorescence biomarkers to identify the stem cells and map their differentiation state. In particular, we mapped the relative concentration of porphyrin and Mouse Embryonic Fibroblasts (MEFs) autofluorescence to distinguish differentiating from undifferentiated hES. Finally, we confirmed these results with classical immunostaining technique.

Applying the phasor approach to FLIM in label-free tissues provides a new tool to characterize local microenvironment and to monitor differentiation and proliferations of stem cells and cancer cells in vivo.

Chapter 1

INTRODUCTION

1.1 Pluripotent Stem Cells

Stem cells are unique cells capable of self-renewal and they have the capacity to give rise to at least one, and sometimes many, specialized cell types. These stem cells are present in many tissues of adult animals and are important in tissue repair and homeostasis. Stem cells belong to different categories depending on the type or types of cells they are able to generate. For example, spermatogonial stem cells in the testis are *unipotent* and produce only one type of differentiated cell (a spermatozoon). Instead, haematopoietic stem cells are *multipotent* and produce erythrocites and all the types of white blood cells. Finally, *pluripotent* stem cells can form theoretically every kind of cell in the animal body and they are not derived from adult but rather from embryonic tissues [7]. Recently, induced pluripotent stem cells (iPS) have been developed through the reprogramming of adult human cells [4][5].

The hallmark of stem cells is their ability to self-renew while generating daughter cells which are committed to differentiate and to form specialized tissues [7]. The modulation of the balance between self-renewing divisions and differentiation is a central mechanism during early embryo development, adult tissue regeneration and homeostasis [8][9]. Tissue development through stem cell differentiation is a complex process mediated both by intrinsic molecular mechanism and extrinsic signaling. The influence of external chemical and physical stimuli on stem cells differentiation and tissue

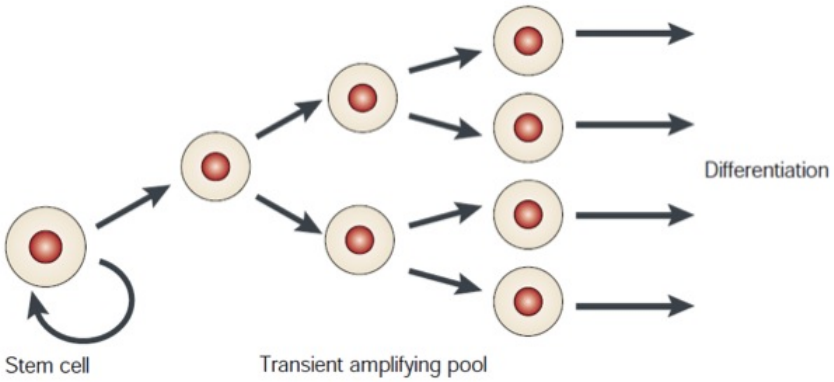

Figure (1.1). *Stem cell differentiation. The pluripotent stem cells can give rise to all cell types in a given organ. They have the big potential of being self-renewing, stem cells are able to product both differentiating daughters and daughters that maintain stem-cell identity.*

development, i.e. molecular gradients, extracellular matrix remodeling and niches signaling, are still relatively unexplored [10][11][12][13].

There are several methods which can be used to measure stem cells differentiation and to monitor their metabolism, either in vitro or in tissues. These methods are very important for cell sorting, in the perspective of using stem cells for tissue engineering. Some of the most promising studies regards exactly the capability of identifying undifferentiated hembryonic stem cells hES and induced pluripotent stem cells iPS [14].

A very common method is immunostaining and it is able to offer reliable information about cellular processes. However, generally this kind of methods require long and invasive procedures that make the cells unviable and unrecoverable and indeed they are incompatible with in vivo dynamic observations.

Recently, optical non-invasive techniques have been developed to obtain information on cell differentiation and to distinguish between different states of cells and cancerous tissues [15][16][17][18][19][20]. These methods exploit intrinsic autofluorescence of cells and tissues and multi-photon microscopy.

1.2 Two-photon Microscopy and FLIM

Multiphoton microscopy is suitable for high resolution and long term imaging of living cells. The beneficial characteristics are its intrinsic three-dimensional resolution, high penetration depth, negligible out-of-focus photobleaching and reduced photodamage [21]. Autofluorescence in live tissues is generated by endogenous proteins and physiologic fluorophores such as collagen, elastin, porphyrin, retinoids, flavins, nicotinamide adenine nucleotide (NADH), haemoglobin and serotonin. For example, NADH and FAD are the main metabolic coenzymes involved in oxidative phosphorylation and glycolysis and they are indicative of metabolic changes associated with cell differentiation and carcinogenesis [19]. However, two-photon fluorescence alone is not able to assign autofluorescence signal to specific intrinsic molecular sources.

Alternative methods have been proposed to assign autofluorescence to specific tissue components. These methods are spectral imaging and Fluorescence Lifetime Microscopy (FLIM). The fluorescence of organic molecules is

characterized by the emission spectrum and the fluorescence lifetime. The principle component analysis of emission spectra need additional information on the tissue biochemical composition and they are able to separate a limited number of tissue components. Another problem, which hinders the discrimination between intrinsic fluorophores sources by the wavelength of the emission, is the overlapping of emission spectra of different fluorescent species.

Multi-exponential fitting of complex fluorescent intensity decays consists on a fitting procedure which needs a priori assumptions on the biological sample, considering that multiple fluorescent species coexist in the focal volume. The majority of intrinsic fluorophores and proteins are characterized by conformational heterogeneity and have complex lifetime distribution with several exponential components [22]. Hence, the choice of a decay model for the intensity decay fitting is arbitrary. Furthermore, associating specific tissue components to exponential decays is a hard task [23].

The phasor approach we used in this thesis work is able to simplify significantly FLIM analysis, allowing a direct interpretation of intrinsic fluorescence signal of living tissues in terms of physiological relevant fluorophores. The phasor approach applied to FLIM is an innovative approach completely different from fitting of exponentials, able to overcome many of the previous problems. The analysis of FLIM images through the phasor approach does not need any a priori assumption and it is label-free, in vivo and in real-time.

The phasor approach can be successfully applied to analyze FLIM images of stem cells. It showed to be a suitable and optimum tool to measure their stage of differentiation and to monitor metabolic and chemical changes in vivo.

Chapter 2

TWO-PHOTON MICROSCOPY

Fluorescence microscopy is a very important tool among biophysicists and biologists because it enables to achieve information about a biological sample in its natural microenvironment. By using different and specific fluorescent dyes, called fluorophores, different molecules can be identified and observed simultaneously in the same biological sample.

Fluorescence microscopy was invented at the beginning of the last century when microscopists, trying to achieve higher resolutions, were experimenting ultraviolet light on biological samples. In the very beginning, obervations were limited to specimens that are naturally fluorescent; few years later, fluorescent dyes, which are able to stain tissues and cells, were investigated.

When coupled to the optical microscope, fluorescence allowed to study a large number of phenomena in modern biology. After conventional widefiled microscopy, in which the entire specimen was bathed in light, and confocal microscopy, where the use of the pinhole enabled to exclude the out-of-focus fluorescence, now multiphoton microscopy is the most used because of its beneficial characteristics.

Multiphoton microscopy offers several advantages. An intrinsic optical sectioning without the use of pinholes is performed and also the photodamage is reduced. The depth of penetration and the spatial resolution with respect to the confocal microscope result considerably increased. Although two-photon excited fluorescence is usually the primary signal source in multiphoton microscopy, three-photon excited fluorescence [24][25][26][27][28][29]

and second [30][31][32] (SHG) and third-harmonic generation [33][34] (THG) can also be used for imaging. In the last 20 years, the multiphoton microscope underwent an impressive growth, making it one of the most used tools in biological imaging of cells and tissues.

Maria Goppert-Mayer showed that photons of lower energy together can produce excitation similarly obtained by the absorption of a single photon of higher energy [35]. This process is called multiphoton or two-photon excitation.

Two-photon microscopy put into practice the simplest version of the theoretical prediction: two photons, each having the same amount of energy (from the same laser), interact with a molecule and the excitation corresponds to the absorption of a single photon possessing twice the energy.

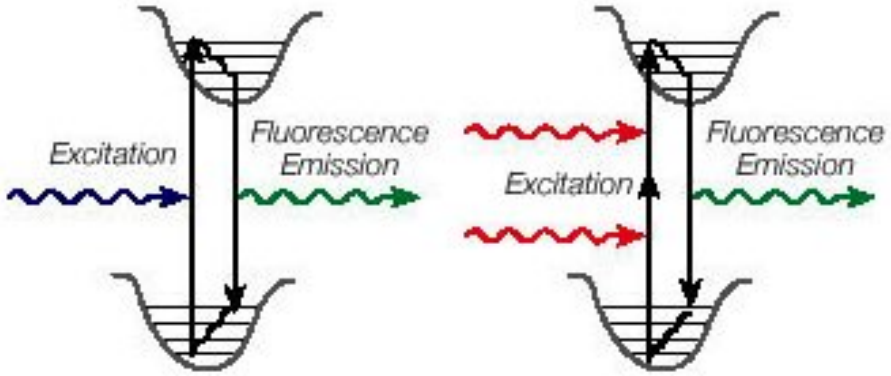

Figure (2.1). *Energy transition for one photon and two photon excitation. Two photons, each having the same amount of energy (from the same laser), interact with a molecule and the excitation corresponds to the absorption of a single photon possessing twice the energy (Slides Enrico).*

A fluorescent excited molecule emits a single photon of fluorescence, as if it were excited by a single higher energy photon. This event occurs because both the two photons interact with the excited molecule nearly simultaneously (about 10^{-16} s). The result is a quadratic dependence on the light intensity rather than the typical linear dependence of conventional fluorescence. Two photon processes are called non linear for this reason: the rate at

which they occur depends non linearly on the intensity of the radiation.The dependence on the intensity is squared and this justifies the localized nature of two-photon excitation: if the intensity is doubled, the fluorescence becomes four times higher.

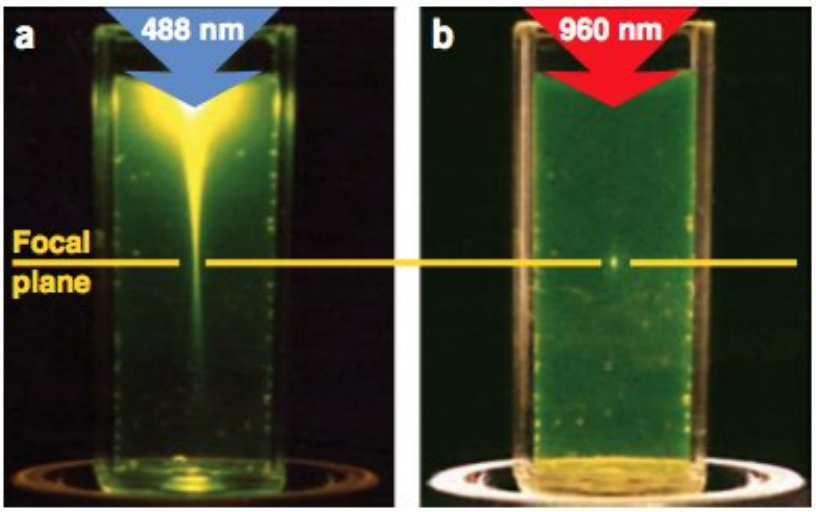

Figure (2.2). *Localization of excitation by two-photon excitation. a) Single photon excitation of fluorescein by focused 488 nm light (0.16 NA). b) Two-photon excitation using focused (0.16 NA) femtosecond pulses of 960 nm light [36]. It can be observed that away from the focal plane the two-photon excitation decreases so rapidly that no appreciable fluorescence is emitted out of the focal plane. In this way three-dimensional resolution is achieved.*

In two-photon microscopy, a laser is focused and raster-scanned through the sample, as in conventional laser-scanning confocal microscopy. The image which is obtained consists of a matrix of pixels, every pixel represents the fluorescence intensity measurement made by digitizing the detector signal as the laser sweeps back and forth across the sample. Since the probabilities of two-photon exciation are very small, focusing is necessary in order to increase the local intensity at the focal point.

The intensity of a radiation is the number of photons passing through a unit area per unit time, whereas the power of the radiation is energy per second. So, intensity depends on the area and it is greater at the focus than

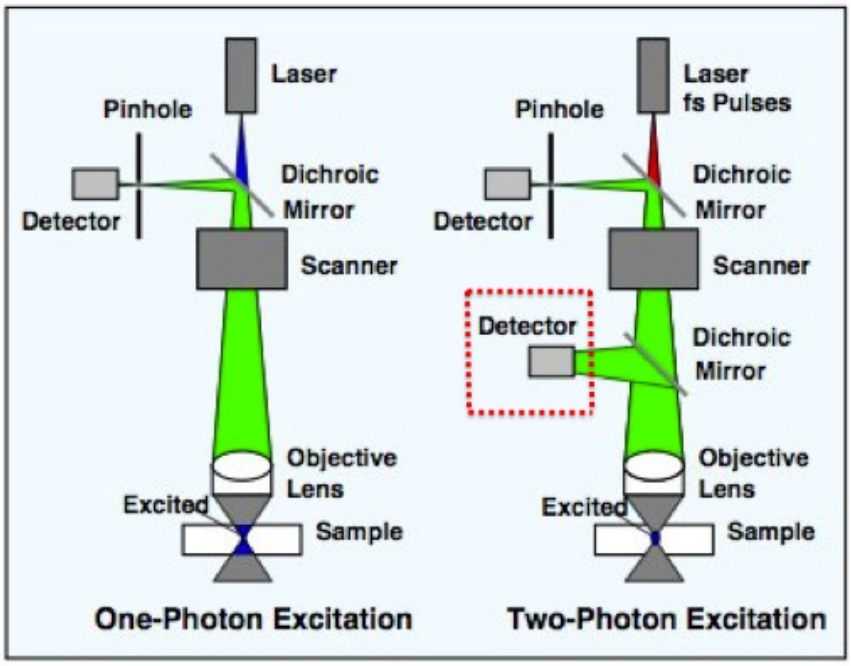

Figure (2.3). *General setup of a laser scanning microscope: one and two-photon excitation [37]. The laser is fed into the optical path via a dichroic mirror and focused into the sample by the microscope objective lens. In the traditional confocal setup for one-photon excitation, the light goes through a pinhole and light from outside the focal plane is not focused. In two-photon microscope, excitation occurs only in the focus, so that no pinhole is required to reject light from outside the focal plane.*

at a distant point, while the total power is equal in every point of the beam. The intensity squared increases the two-photon excitation probability in the focal plane by 10^7 compared to the unfocused beam. Finally, away from the focal plane the two-photon excitation decreases so rapidly that no appreciable fluorescence is emitted out of the focal plane. In this way three-dimensional resolution is achieved.

However, focusing alone is not sufficient to make two-photon microscopy practical. In order to generate two-photon excitation fluorescence that is sufficient for imaging, a pulsed laser is used to increase further the probability that the two photons will simultaneously interact with the molecule. The pulsed laser lets also keep the average power relatively low. The most common laser used in multiphoton microscopy is a mode-locked titanium sapphire (Ti:S) laser. It produces about 80 million pulses per second, each pulse having a pulse duration of about 100 fs.

The two-photon cross-section σ_{2p} is the quantitative measure of the probability of a two-photon absorption. σ_{2p} has units of cm^4 s, with 10^{-50} cm^4 s called a Goppert-Mayer or 'GM'.

The two-photon cross-section is hard to measure directly and so, instead of it, the two-photon 'action' cross-section is usually measured. This 'action' cross-section is calculated as the product of the fluorescence quantum yield ϕ_f and the absolute two-photon absorption cross-section σ_{2p} [28][38][39] . Both the wavelength dependence and the absolute value of the product are relevant. A good rule to determine an optimal two photon excitation wavelength is obtained doubling the maximum single-photon excitation wavelength. Unfortunately, several molecules deviate from this approximation because the selection rules for two-photon processes are different from those for single-photon. Some fluorophores, for example Rhodamine B [39], show a clear difference between their one and two-photon absorption spectra.

In Fig. 2.4 we can observe the two-photon action cross section of common biological molecules. When the wavelenght increases, the two-photon action cross section of NADH becomes very low.

The intrinsic fluorophores in tissues have a wide action cross section values. For example NADH molecules have an extremely low 'action' cross section ($< 10^{-4}$ GM) and they have been successfully used with multiphoton

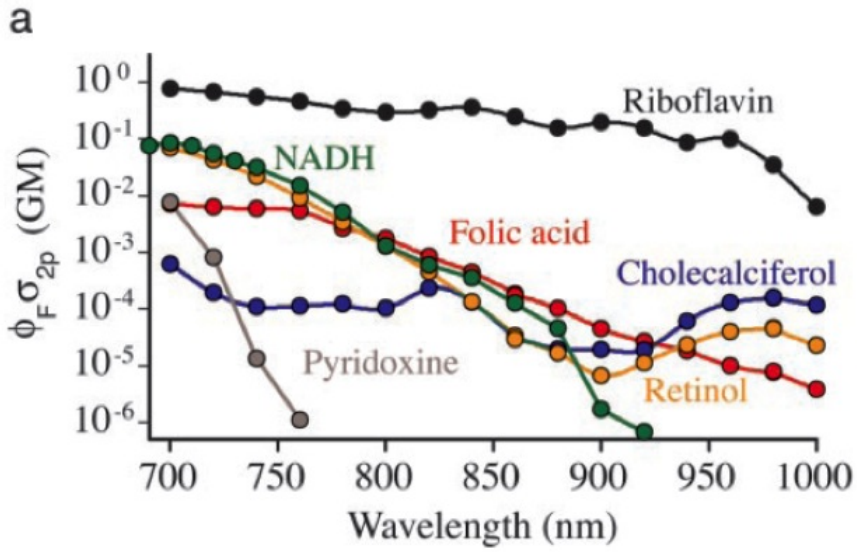

Figure (2.4). *Two-photon action cross-section. The two-photon cross-section σ_{2p} is the quantitative measure of the probability of a two-photon absorption. The 'action' cross-section is calculated as the product of the fluorescence quantum yield ϕ_f and the absolute two-photon absorption cross-section σ_{2p}. (A) Two-photon action cross sections from a basic set of biological molecules [36].*

imaging [40]. At the opposite side, some molecules, like CdSe-Zns quantum dots, have cross-sections of about 50,000 GM [41] and thus they allow multiphoton imaging with a very low laser power (few microwatts). However, besides extreme cases, most common fluorescence dyes have $\phi_f \sigma_{2p}$ values in the range 1-300 GM [28][39]. It is also possible to design organic molecules specifically for high nonlinear absorption [42][43]. Intrinsically fluorescent proteins, such as GFP (green fluorescent protein), have large 'action' cross-sections values [28] and are particularly suited for two-photon microscopy in tissue explants and live animals [44][45][46][47][48].

Although relative two-photon excitation spectra (depends on λ) are useful [49][50], in order to design a successful multiphoton experiment it is often required to know $\phi_f \sigma_{2p}(\lambda)$ explicitly. Otherwise, it could happen that the relative excitation spectra alone do not provide the needed information, and an absolute measure of the expected fluorescence from each species at a given wavelength is necessary.

Chapter 3

FLUORESCENCE LIFETIME MICROSCOPY

3.1 Introduction

Fluorescence is a sensitive technique that provides a crucial contrast enhancement in microscopic imaging.

Fluorescence microscopy allows labeling biological samples with high specificity, giving an excellent background rejection. It spatially resolves with a strong contrast microscopic structures of interest, such as cellular components. Besides the detection of the spatial relationship of the cellular organelles, fluorescence microscopy is fundamental in understanding the cellular physiology because it can reveal important parameters, such as the pH or molecular concentration. Moreover, fluorescence probes are very sensitive to cellular microenvironment, some of them are fluorescent only with specific polarity condition or pH. According to all these reasons, fluorescence intensity measurements are used to monitor processes in cells and tissues but sometimes they are not sufficient to give quantitative information. As a matter of fact, the fluorescence intensity depends either on the fluorophore environment and on the local probe concentration, and the two contributions cannot be easily discriminated.

However, the fluorescence of organic samples is not only characterized by the emission spectrum, it has also a characteristic lifetime. Any energy

transfer between an excited molecule and its microenvironment changes the lifetime in a predictable way. Since the lifetime does not depend on the concentration of the chromophore, fluorescence lifetime imaging is a direct approach to all effects that involve energy transfer. Techniques that feat either spectral-sensitive and lifetime-sensitive probes can be used to measure quantitatively environmental factors that affect the excited state and to identify intrinsic molecular sources [51][52][53][54][55]. Hence, spectral and fluorescence lifetime techniques coupled to fluorescence microscopy can give quantitative information of the cellular and tissue environments. The fluorescence lifetime of a molecule is the average amount of time that elapses before the excited molecule returns to the ground state. This lifetime is affected by any energy transfer process between the excited molecule and its environment. Therefore, fluorescence techniques are able to reveal information about the molecular state of a chromophore but, to achieve a more complete investigation of the nature of molecular interaction, time-resolved measurements are required. A way to determine the nature of molecular interactions consists of measuring the probe's fluorescent lifetime.

The sensitivity of fluorescence lifetime to the microenvironment has been used to measure pH [56], metal ion concentration [57][58], fluorescence resonance energy transfer [59][60] , cellular photostress [61] and antigen processing [62]. Other quantities that can be measured by lifetime imaging techniques are molecular oxygen concentration, environmental polarity and local order. Besides, different fluorophore species, having different lifetimes, can be represented in one picture, and a single image element can resolve each fluorophore's fraction [63][64].

Time resolved fluorescence microscopy has been applied firstly with single-pixel measurements [65][66] and the first experiments provided important cellular information such as calcium concentration or cytoplasm matrix viscosity at selected positions within a cell. Later, the advancement in fluorescence lifetime resolved microscopy consisted of the extension of single-point measurements to obtain lifetime information across the whole cell. This has been possible through two different approaches: the first using CCD cameras equipped with gain-modulated image intensifiers and the second one through traditional confocal laser scanning microscopes modified in order to

obtain time-resolved information on a point-by-point basis. The laser scanning microscopy has been used to measure three-dimensionally resolved lifetime images with confocal detection [67][68], two photon excitation [69][63] and time-dependent optical mixing [70][71]. Also near-field scanning optical microscopy has been used to image surface fluorescent lifetimes [72][73].

Fluorescence lifetime imaging can been achieved using two functionally equivalent methods. In the first method, known as time-domain technique, the response of the system to an $impulse$ source is measured to obtain information about the fluorescence decay [74][59][75]. In the second one, the so-called frequency-domain technique, the response to a $harmonic$ excitation source is analyzed [76][77][78][79] . Although the time domain and the frequency domain techniques are theoretically equivalent, practically the corresponding recorded signals are different. Hence, the two techniques have different benefits and drawbacks and shall thus be used according to the type of measurements one wants to achieve.

3.2 Fluorescence Lifetime Theory

The fluorescence lifetime of a molecule is the average amount of time that elapses between the excitation state of a molecule and its return to the ground state.

Even if fluorescence lifetime is usually referred to the properties of fluorophores as if they were in isolation, in reality the processes of absorption and emission are studied on populations of molecules and the different properties of the members of the population are revealed by the macroscopic properties of the process.

The decay rate of an initially excited population of molecules is described by the following rate equation:

$$\frac{dN(t)}{dt} = -\left(\Gamma + k\right) N(t) + f(t) \tag{3.1}$$

where N(t) is the number of excited molecules at time t, Γ and k are the radiative and non-radiative decay rate constant, and f(t) is an arbitrary function of time describing the time necessary to the excitation of the molecules.

The dimensions of Γ and k are sec^{-1} and they indicate two substantially different processes. The radiative decay rate constant Γ represents the rate of the emission process, hence it is characteristic of the specific fluorophore molecule. Instead, the nonradiative decay rate constant k is the sum of the rates of all other deactivation processes that occur, so it depends on the fluorophore's interaction with the local environment.

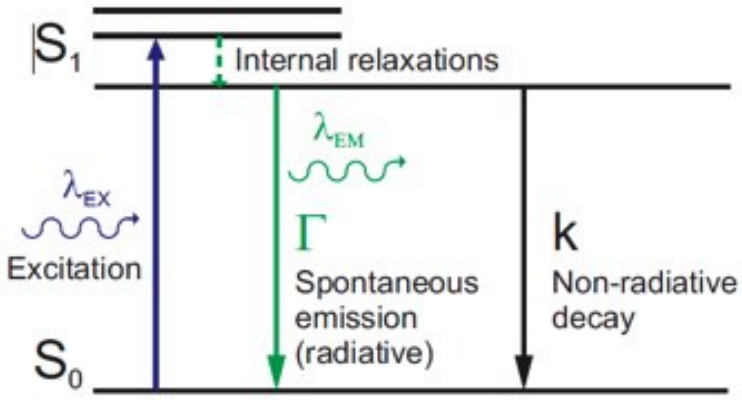

Figure (3.1). *Energy diagram of the absorption-emission process. The radiative decay rate constant Γ represents the rate of the emission process,hence it is characteristic of the specific fluorophore molecule. The nonradiative decay rate constant k is the sum of the rates of all other deactivation processes, so it depends on the fluorophore's interaction with the local environment.*

If the excitation starts at $t = 0$, the decay equation becomes:

$$\frac{dN(t)}{dt} = -(\Gamma + k)\, N(t) \tag{3.2}$$

The integration of the equation 3.2 with the initial conditions $N(t = 0) = N_0$ gives:

$$N(t) = N_0\, e^{-\frac{t}{\tau}} \tag{3.3}$$

where

$$\tau = \frac{1}{\Gamma + k} \tag{3.4}$$

and τ is the lifetime of the excited state. When a population of fluorophores is excited, the lifetime is the time it takes for the number of excited molecules to decay to $\frac{1}{e}$, or 36.8% of the original population, according to:

$$\frac{N(t)}{N_0} = e^{-\frac{t}{\tau}} \tag{3.5}$$

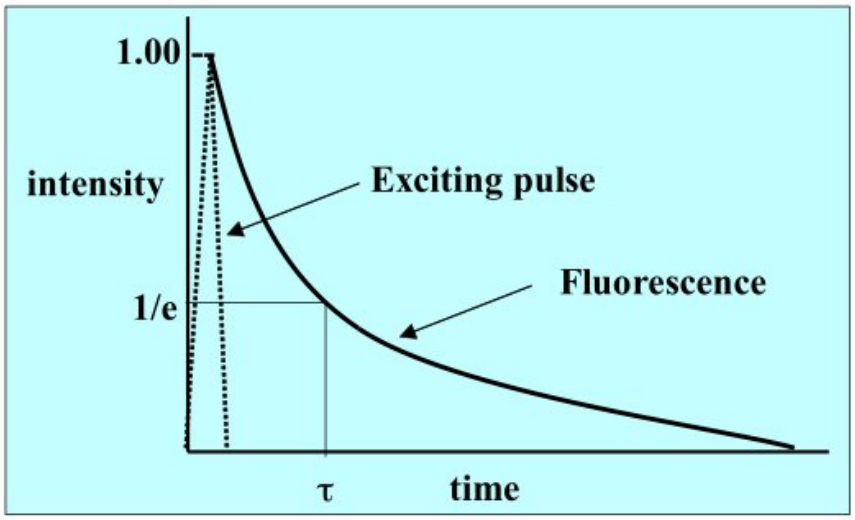

Figure (3.2). *Representation of equation 3.5: exciting pulse and exponential decay of the fluorescence of the excited population. The lifetime τ is the time it takes for the number of excited molecules to decay to $\frac{1}{e}$.*

Hence, as it is clear from the figure 3.2, we expect that the fluorescence intensity $I(t)$ decays exponentially. Applying the definition of the lifetime (average time it takes for the population of excited molecules to return to the ground state), we obtain mathematically:

$$\langle t \rangle = \frac{\int_0^\infty tN(t)dt}{\int_0^\infty N(t)dt} \tag{3.6}$$

Since N(t), as we already said, has an exponential decay,then:

$$\langle t \rangle = \frac{\int_0^\infty t N_0 \, e^{-\frac{t}{\tau}} dt}{\int_0^\infty N_0 \, e^{-\frac{t}{\tau}} dt} \tag{3.7}$$

with

$$\langle t \rangle = \tau \tag{3.8}$$

In conclusion, the average period of time in which a molecule remains in its excited state is equal to the fluorescence lifetime.

The fluorescence lifetimes of typical fluorophores used in cell imaging are of the order of a few ns and it is very important to remember that the lifetime of a given fluorophore is strongly affected by its microenvironment. One clear example of this aspect is the behavior of NADH: in water it has a lifetime of about 0.4 ns while if it is bound to dehydrogenases the lfetime becomes 9 ns.

3.3 Time-Correlated Single Photon Counting

In the time domain method, the impulse response of a system is detected. A fluorescent sample is flashed many times by a narrow pulse of light, and the consequent fluorescence emission decay is measured by a fast recorder.

The most common method used to reconstruct the decay curve is the Time-Correlated Single-Photon Counting (TCSPC) technique. This method records the time delay between the excitation pulse and the emitted photon. Every photon's delay can be recorded if the emission rate is low enough (that means fewer than 10^5 photons per second). Then, the entire decay profile is reconstructed through the plot of the number of photons as a function of the delay times. Besides, in order to reconstruct the decay curve without artefacts, the excitation profile has to be measured and it can be used to obtain through deconvolution the finite width of the excitation pulse from the emission profile.

In the TCSPC method, the fluorescence sample is excited by a pulsed laser, a typical repetition rate is 80 MHZ. The emitted photons are recorded by a fast PMT, MCP or a single photon avalanche photodiode. In order to get accurate measurements, these detectors allow count rates of the order of a few MHZ, much less than the laser repetition rate. In this technique, the excitation pulse must be much shorter than the decay we want to measure. The

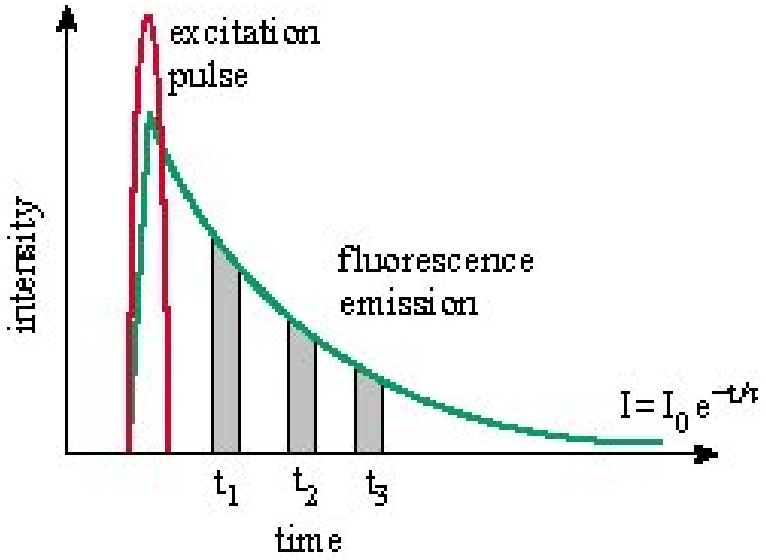

Figure (3.3). *In time domain techinques a sample is illuminated several times by a short laser pulse. The histogram of the time intervals between the excitation and the first emitted photon is represented.*

TCSPC method is intrinsically digital; in fact the detector counts one photon at time. However, in order to measure the time delay, an analog detection method (time to amplitude converter) is used and it is followed by fast conversion to digital form. Hence, only one photon is collected for every pulse and the next pulse cannot arrive before the decay is completely finished.

The TCSPC method takes advantage of the fact that the detection of multiple photons in one laser period is small enough to be neglected. So, when one photon (which is the first photon emitted by the sample) is detected, the delay of the corresponding detector pulse in the laser pulse sequence is recorded. These measured times are used to address a histogram memory in which the photons are accumulated. After a large number of pulses of the laser, the photon density as a function of time is reconstructed in the memory.

The main benefits of the TCSPC method are a near-ideal counting efficiency and an ultra-high time resolution. Moreover, there is no loss of photons until the count rate is low enough to allow an appropriate conversion time of the measurement for the histogramming procedure. The factors that limit the

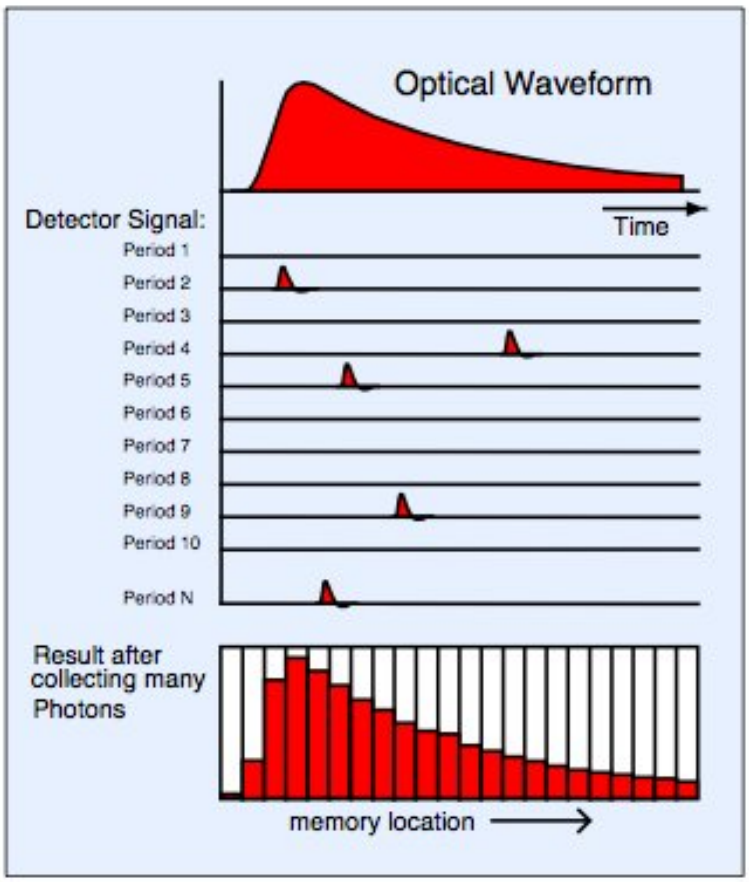

Figure (3.4). *Representation of the principle of Time-Correlated Single-Photon counting. TCSP method consists of recording the time delay between the excitation pulse and the emitted photon. The entire decay profile is reconstructed through the plot of the number of photons as a function of the delay times [37].*

resolution of this technique are the accuracy of the measurement, the transit time spread in the detector and the timing accuracy of the discriminator that receives the detector pulses. The TCSPC method is often considered very slow and so unable to reach short acquisition time. Anyway, high count rate techniques exist since the late 80's [80]. In [51] an early implementation of the TCSPC technique in a microscope is described.

To obtain the images, TCSPC Imaging is the advanced technique that is used in conjunction with Scanning Microscopes. This technique reconstruct a 3-D histogram of the number of photons as a function of the time and of the coordinates of the scan area. For this method, the recording electronics requires a time measurement channel, a scanning interface and of course a large histogram memory. In the following figure, the comparison between two images obtained with the TCSPC technique are represented. The first one is the image of a fluorophore having a single-exponential lifetime, while the second one is an image obtained from a tissue.

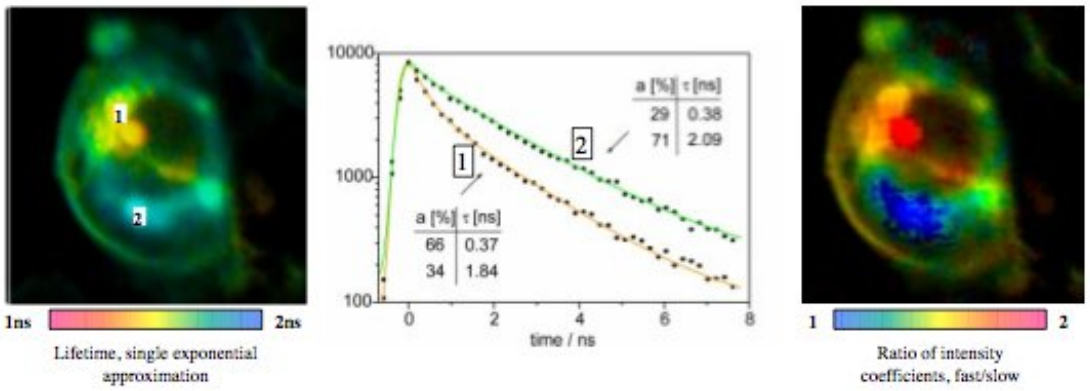

Figure (3.5). *Example: HEK cell containing CFP and YFP in the* $alpha$ *and* $beta$ *subunits of the sodium channels. Left: Lifetime image of donor, CFP, centre: Decay curves of selected pixels, right: FRET image showing ratio of intensity coefficients of quenched and unquenched fluorescence components. Data from [37], Zeiss LSM-510, Becker Hickl SPC-730.*

3.4 Frequency Domain Measurements

The frequency domain method measures the harmonic response of a system. A sinusoidally modulated source excites the sample and the emission signal is still a sine wave but it is modulated and phase shifted respect to the source. Both the modulation and the phase shift can be used to determine the fluorescence lifetime.

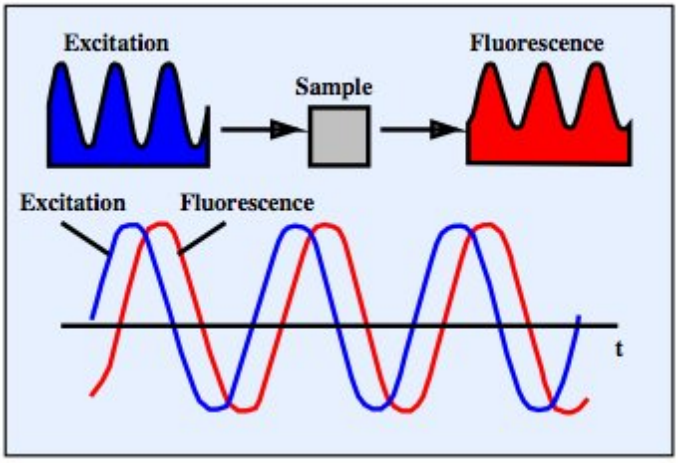

Figure (3.6). *Modulation technique. A sinusoidal source excites the sample and the emission signal is still sinusoidal but it is modulated and phase shifted respect to the source. The modulation and the phase shift are used to calculate the fluorescence lifetime. [37].*

In a modulation technique, the excitation frequency is described by the function:

$$E(t) = E_0(1 + M_E sin(\omega t)) \tag{3.9}$$

where E(t) and E_0 are the intensities respectively at time t and 0, M_E is the modulation factor (related to the ratio of AC and DC components of the signal) and ω is the angular modulation frequency or 2π times the repetition frequency f.

The figure 3.7 illustrates the phase delay ϕ and the modulation that arise between the excitation E(t) and the emission F(t), due to the persistence of

the excited state. The AC and DC levels associated with the excitation and the emission waveforms are also represented.

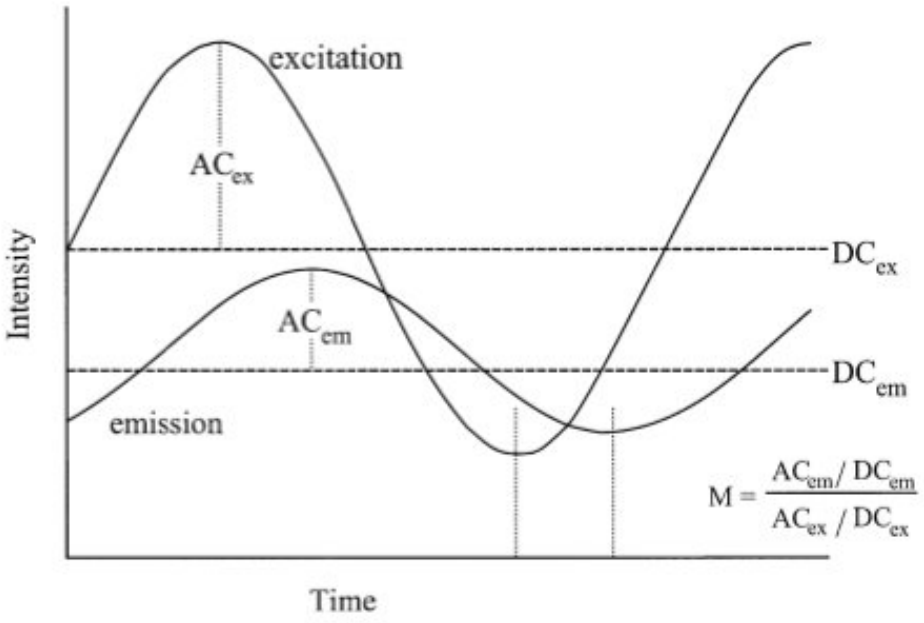

Figure (3.7). *In frequency domain techniques a specimen is excited by a modulated light source. The fluorescence emission has the same frequency of the excitation source but it results modulated and phase shifted [81].*

It can be demonstrated that:

$$F(t) = F_0(1 + M_F sin(\omega t + \phi)) \tag{3.10}$$

Hence, the phase ϕ and the modulation M are related to the fluorescence lifetime τ. For a single exponential decay, the two following equations can be demonstated:

Phase equation:

$$\phi = \tan^{-1} \omega\tau \tag{3.11}$$

Modulation equation:

$$M = \frac{1}{\sqrt{1 + \omega^2\tau^2}} \tag{3.12}$$

Using the phase shift ϕ and the relative modulation M, also the phase lifetime τ_ϕ and modulation lifetime τ_M can be determined:

$$\tau_\phi = (\frac{1}{\omega}) \tan \phi \tag{3.13}$$

$$\tau_M = \frac{1}{\omega}(\frac{1}{M^2} - 1)^{\frac{1}{2}} \tag{3.14}$$

If the fluorescence decay is a single exponential, τ_ϕ and τ_M are equal for every modulation frequency. Instead, in the case of multi exponential decay τ_ϕ and τ_M and their values depend on the modulation frequency, for example:

$$\tau_\phi(\omega_1) < \tau_\phi(\omega_2) \tag{3.15}$$

if

$$\omega_1 > \omega_2 \tag{3.16}$$

As we saw, both the phase and the modulation can be used to determine the fluorescence lifetime. However, phase measurements are generally much more accurate and therefore they are normally preferred. For maximum sensitivity, the angular modulation frequency has to be roughly the inverse of the lifetime:

$$\omega\tau = 1 \tag{3.17}$$

Since fluorescence lifetimes are of the order of nanoseconds or picoseconds, a modulation frequency between 50 MHz and 100 MHz is used. Besides, phase measurements at different frequencies are necessary to resolve the components of multi-exponential decay functions.

For frequencies between 100MHz and 1 GHz, the time resolution of a frequency domain method is in the ps range. For one-photon excitation the light

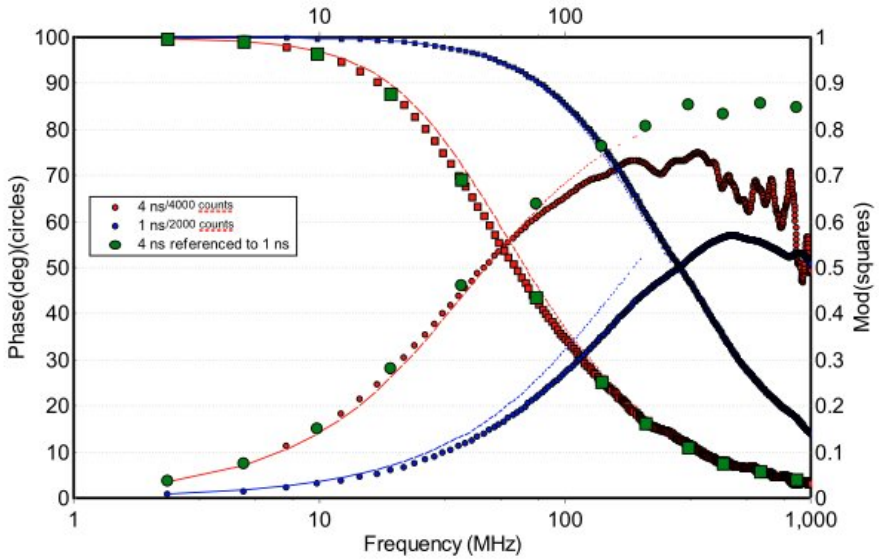

Figure (3.8). *Multi exponential decay of a system with two different life-times. Frequency-domain representation after fast Fourier transformation of the data. The red spots are the 4 ns component (4000 counts), the blue spots represent the 1 ns component, the green spots represent the 4 ns components referenced to the 1 ns component. Eq. 3.13 and 3.14 were used [82].*

source can be a modulated laser diode or a CW laser with an external modulator. Instead, for two-photon excitation a Ti:Sa laser is used and the phase is measured at the fundamental pulse frequency of the laser and at its harmonics.

Chapter 4

PHASOR ANALYSIS OF FLIM

4.1 Introduction

Fluorescence Lifetime Imaging Microscopy (FLIM) is a fundamental technique in microscopy and it has been demonstrated to be an extremely useful tool to achieve quantitative analysis of biological samples.

The outcomes of fluorescence experiments are intensity decay profiles. They are originated by the lifetime contribution of the different molecular species existing in the sample, each one of them having multiple lifetime components [83][84]. Also different conformations of the same molecule create different decay curve because molecular interactions change the lifetime values [85][86]. Several methods can be used to measure the fluorescence decay in FLIM, two techniques have been described in the previous chapter: the time-correlated single photon counting and the frequency-domain method.

However, in FLIM there are some technical challenges concerning data acquisition and also data analysis and interpretation.

Firstly, at every pixel of the image contributions of several fluorescent species are present, and each one of them can be multi-exponential. Besides, it is possible to collect the light just for a limited amount of time (100-200 μs per pixel) and this results in a small amount of photons for every pixel (500-1000) [82]. This number of photons is barely enough to distinguish even a double exponential from a single exponential decay with multiple exponential fitting.

The common way to analyze FLIM data collected in time domain consists of fitting the decay profile at every pixel using one or more exponential functions in order to match the different molecular species and their relative quantities with the correspondent decay times and amplitudes. This approach leads to several problems. Many of the fluorescent proteins usually used in microscopy give rise to very complex decay profiles [87]. Moreover, in exponential functions there is correlation between the amplitudes and the exponential times. In a typical image there are about 10^5 pixels and resolving the decay at each pixel requires to fit a function, this is a complex computational task that can be done only by experts [88],[89]. Substantially, the approach of exponentials fitting has many limitations: it depends on the initial conditions used and on the hypothesis made on the sample; a proper interpretation of the multi-exponential decay is complex and the number of fitting parameters is high; the fit is very slow.

The phasor approach applied to FLIM is an innovative approach completely different from fitting of exponentials, able to overcome many of the previous problems. The phasor approach uses a different representation of the decay where each molecular species has its own unique identification and each process (like FRET or ion concentration changes) can be easily recognized. The phasor approach gives many simplifications and advantages. The decay of each pixel is represented in a graphical global view [90],[91] and the algorithm used is fit-free and it doe not require a priori knowledge on the system. Every chemical species has its own "fingerprint" and so complex systems can be interpretate straigthforward: the contribution of every different species can be recognized and quantificate. All this can be done through a fast analysis.

4.2 Phasor Transformations

The phasor approach can be applied to every technique that acquires fluorescence lifetime images, such as time correlated single photon counting (TCSPC) and frequency domain methods. The phasor approach works in a new "space", where each decay component or molecular species is identified by a unique vector in the "phasor plot". This special vector is called phasor and its

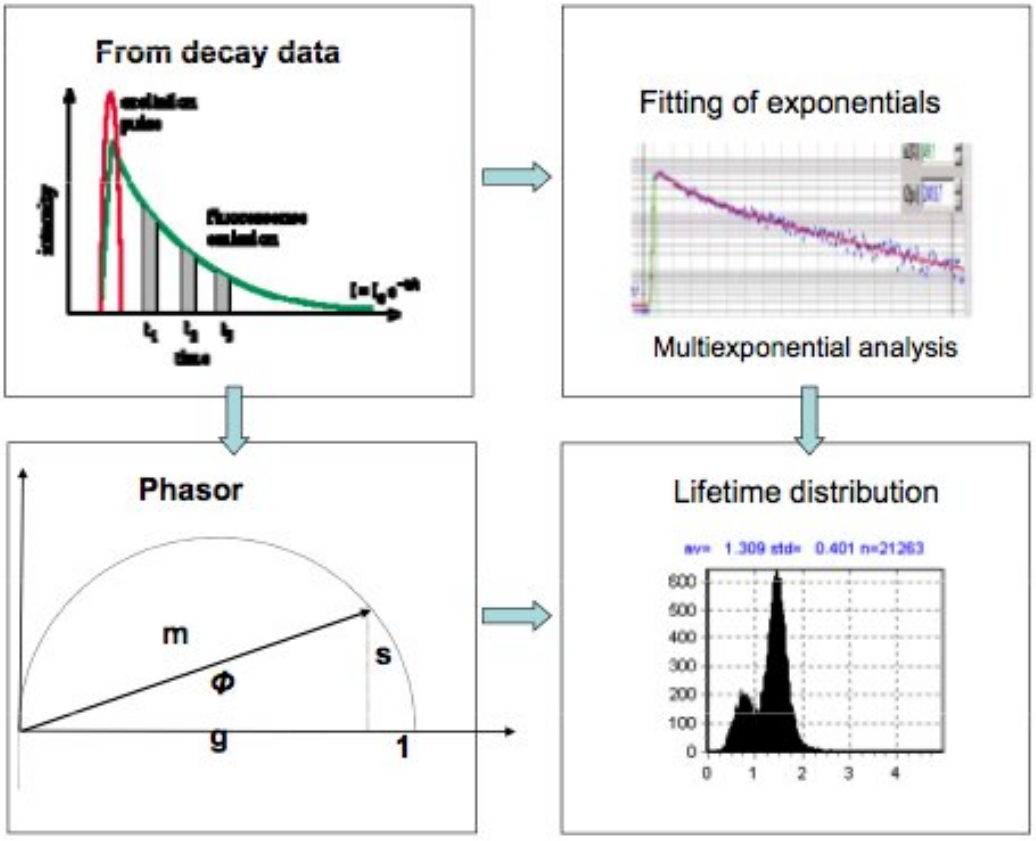

Figure (4.1). *Comparison between fitting of exponentials and phasor approach. The phasor approach applied to FLIM is an innovative approach which is able to overcome the typical problems of the fitting exponentials method. The phasor approach is a fit-free graphical algorithm, able to identify an unlimited number of components. It allows a straightforward interpretation of data and a fast analysis of the image.*

location in the phasor plot is unique, irrespective of the number of exponentials needed for the description of the fluorescence intensity decay.

A phasor, being a quantity analogous to a vector, is described by a module M and a phase ϕ.

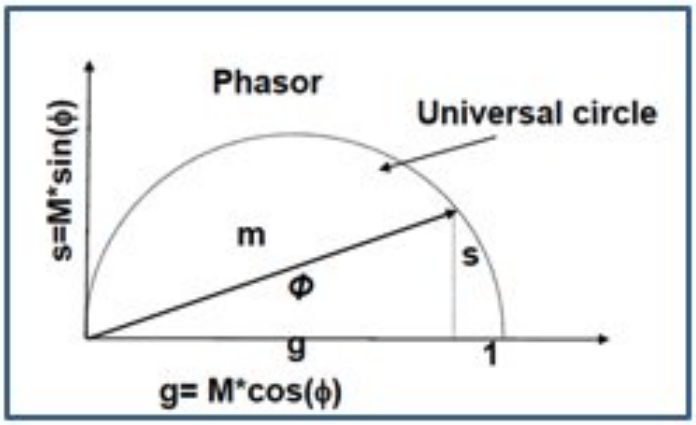

Figure (4.2). *Graphical representation of a phasor in the phasor plot. The universal circle and a phasor are represented. The phasor is identified by its module M and its phase ϕ. g is the x-coordinate of the phasor and s is the y-coordinate of the phasor in the phasor plot.*

As represented in the previous figure, the x and y coordinates of the phasor in the phasor plot are respectively:

$$g = M\cos\phi \tag{4.1}$$

$$s = M\sin\phi \tag{4.2}$$

Estimations of the average lifetime in terms of the phase and modulation can be performed in each pixel by the following formulas:

$$\tau_\phi = \frac{1}{\omega} tan(\phi) \tag{4.3}$$

$$\tau_m = \frac{1}{\omega}\sqrt{(\frac{1}{m^2} - 1)} \tag{4.4}$$

The theoretical equations that transform the intensity decay in the x and y coordinates, permitting us to work in the phasor plot, are different for time domain and frequency domain techniques. Assume to have an intensity decay I(t) acquired with a time domain method. The g and s coordinates corresponding to the decay profile I(t) are given by the following equations:

$$g_{i,j}(\omega) = \frac{\int_0^\infty I_{i,j}(t)\cos(\omega t)\,dt}{\int_0^\infty I_{i,j}(t)\,dt} \tag{4.5}$$

$$s_{i,j}(\omega) = \frac{\int_0^\infty I_{i,j}(t)\sin(\omega t)\,dt}{\int_0^\infty I_{i,j}(t)\,dt} \tag{4.6}$$

where ω is the laser repetition angular frequency and the indexes i and j identify a pixel of the image.

In the second case, if the data are acquired in the frequency domain, the equations used to obtain g and s are the following:

$$g_{i,j}(\omega) = M_{i,j}\cos(\phi_{i,j}) \tag{4.7}$$

$$s_{i,j}(\omega) = M_{i,j}\sin(\phi_{i,j}) \tag{4.8}$$

where $M_{i,j}$ and $\phi_{i,j}$ are respectively the modulation and the phase of the emission light with respect to the excitation light source.

In the case of a single exponential, the two separate lifetimes obtained by the phase and the modulation with Equation 4.7 and 4.8 are equal, while for a multi exponential lifetime system the apparent lifetimes are different. In the phasor plot, if the decay is single exponential:

$$I(t) = A\,e^{-\frac{t}{\tau}} \tag{4.9}$$

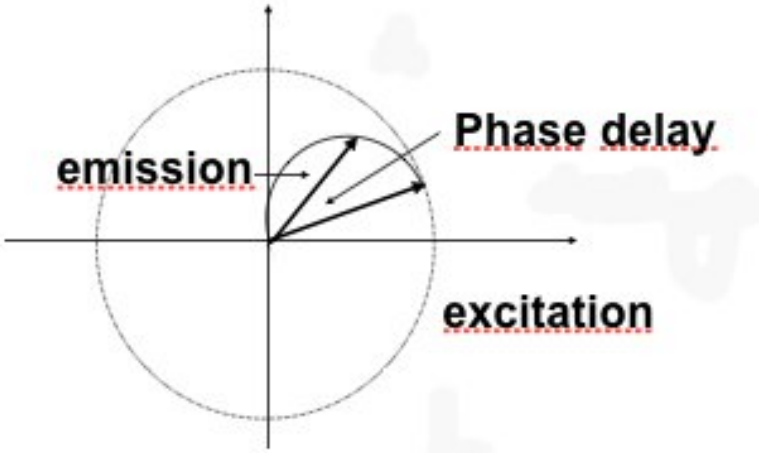

Figure (4.3). *Representation of phase delay and modulation between the excitation and the emission source, associated to the phasor behavior.*

it means that only one molecular species is present in a certain pixel.
The coordinates of the phasor are given by:

$$g_{i,j}(\omega) = \frac{1}{1 + (\omega\tau)^2} \tag{4.10}$$

$$s_{i,j}(\omega) = \frac{\omega t}{1 + (\omega\tau)^2} \tag{4.11}$$

where τ is the lifetime of the decay and ω is the laser repetition frequency.
Instead, if the decay is multi exponential:

$$I(t) = \sum_i a_i \, e^{-\frac{t}{\tau_i}} \tag{4.12}$$

several molecular species contribute to the decay profile of a certain pixel, and the coordinates of that pixel in the phasor plot are given by:

$$g_{i,j}(\omega) = \sum_k \frac{f_k}{1 + (\omega\tau_k)^2} \tag{4.13}$$

$$s_{i,j}(\omega) = \sum_k \frac{f_k \omega \tau_k}{1 + (\omega \tau_k)^2} \tag{4.14}$$

where f_k is the intensity weighted fractional contribution of the molecular species with a certain lifetime τ_k. Recalling the equations of the coordinates for a single exponential decay, we obtain:

$$\left(g_{i,j} - \frac{1}{2}\right)^2 + (s_{i,j})^2 = \left(\frac{1}{2}\right)^2 \tag{4.15}$$

The previous equation implies that all single exponential lifetimes lie in the semicircle centered in $\left(\frac{1}{2}, 0\right)$ with radius $\frac{1}{2}$. This semicircle is called the "universal circle". As the modulation frequency increases, the end of the phasor describes the "universal circle". To give an idea, a phasor with a small phase angle value corresponds to a very short lifetime ($\tau \approx 0$) and it lies close to the point $(1, 0)$. Instead, a phasor with a bigger phase angle corresponds to a long lifetime ($\tau \approx \infty$) and it lies close to the point (0,0).

It has been said previously that the phasor approach applies both to data acquired in the time domain and in the frequency domain. In the following figures, the plots and the equations needed to calculate the phase and the modulation in the time domain and in the frequency domain are represented. The plots are different (because of the totally different acquisition modes) but the equations used are exactly the same. Even if the theoretical transformations are indeed different, in the practice the calculation of the phasor requires the same equations for the time and the frequency domain.

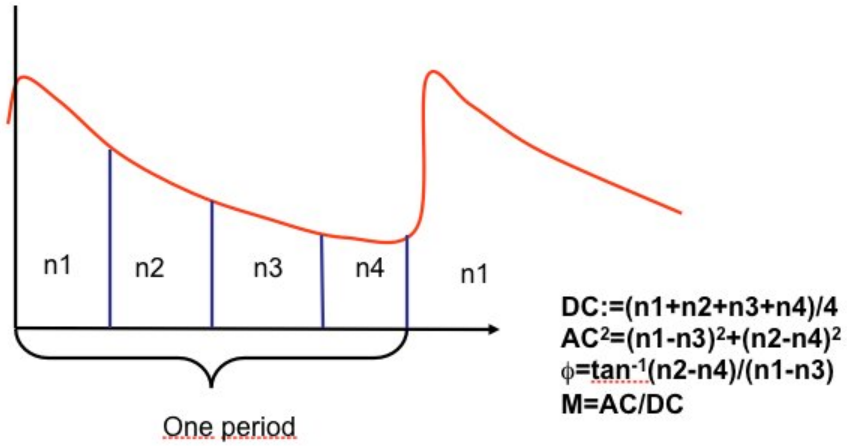

Figure (4.4). *Calculation of phase and modulation of the phasor for time domain techniques. Four values (n1, n2, n3 and n4) are identified in the time decay profile and they are used to calculate the phase ϕ and the module M of the phasor.*

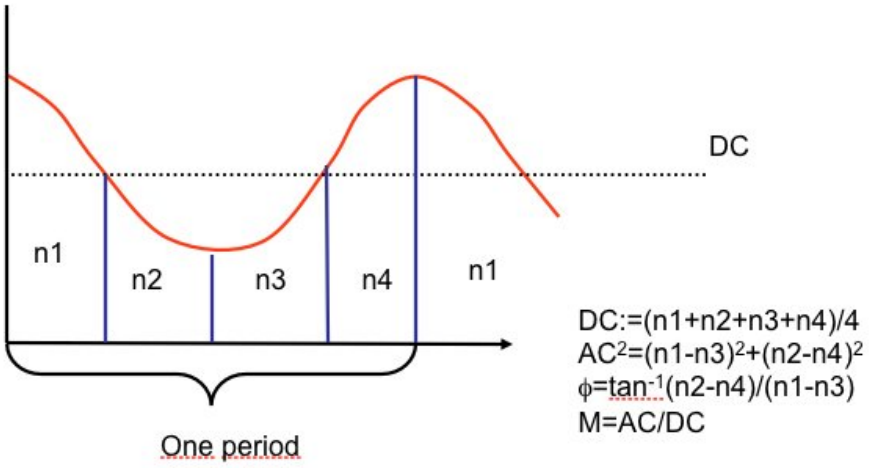

Figure (4.5). *Calculation of phase and modulation of the phasor for frequency domain techniques. Four values (n1, n2, n3 and n4) are identified in the sinusoidal emission signal and they are used to calculate the phase ϕ and the module M of the phasor.*

4.3 Phasor Rules

The phasor plot is a new coordinate system where the single lifetime components add linearly to originate the total measured intensity decay. In fact, since the phasors are quantity like vectors, the sum of the phasors consists of the sum of vectors. The vector components need to be calculated and added to obtain the vector sum.

All single exponential lifetimes lie on the "universal circle" but usually an ensemble of fluorescent species does not decay with a single lifetime. Therefore, if multiple fluorescent species are present, each emitting with more than one lifetime or a distribution of lifetimes, the points on the Phasor Plot corresponding to each separate fluorescent species will not lie on the semicircle.

Assume to analyze the simple case of a molecular species whose decay profile has the contribution of two lifetimes τ_1 and τ_2. Multi exponential lifetimes are a linear combination of their components, hence all possible weighting of the two species characterized by τ_1 and τ_2 must be on the straight line joining the locations of the two single lifetime. The ratio of the linear combination determines the fraction of the components (fraction intensity) f_2 and f_1 and identifies the exact location of the molecular species phasor.

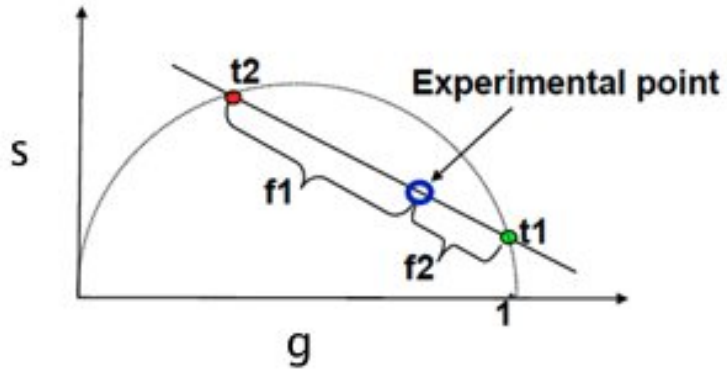

Figure (4.6). *Phasor of a mixture of two single lifetime τ_1 and τ_2. The phasor of the mixture is a linear combination of τ_1 and τ_2 and so it lies on the line joining the phasors of the two components.*

So, every molecular species has a specific location in the phasor plot. This

identification between species and phasors can be considered a "phasor fingerprint".

This phasor position is determined by the intrinsic characteristics of its fluorescence decay. For example, different chemical species A, B, C, D in Fig. 4.7 have their different specific location in the phasor plot.

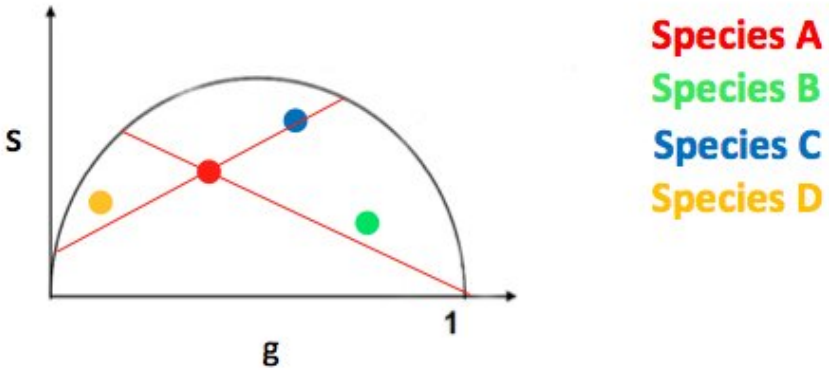

Figure (4.7). *Example of "phasor fingerprints" in the phasor plot for different molecular species. Every molecular species has a specific location in the phasor plot. This identification between species and phasors can be considered a "phasor fingerprint".*

In Fig. 4.7, we can observe that the species A (red species) can be a linear combination of different lifetimes. The two lines represent two examples.

In general, in a system with multiple fluorescent components like a tissue, the overall decay is a phasor which is the sum of the independent phasors of each fluorescent component:

$$G(\omega) = \sum_n f_n g_n(\omega) \tag{4.16}$$

$$S(\omega) = \sum_n f_n s_n(\omega) \tag{4.17}$$

where f_n is the fractional contribution of each component characterized by the phasor coordinates g_n and s_n.

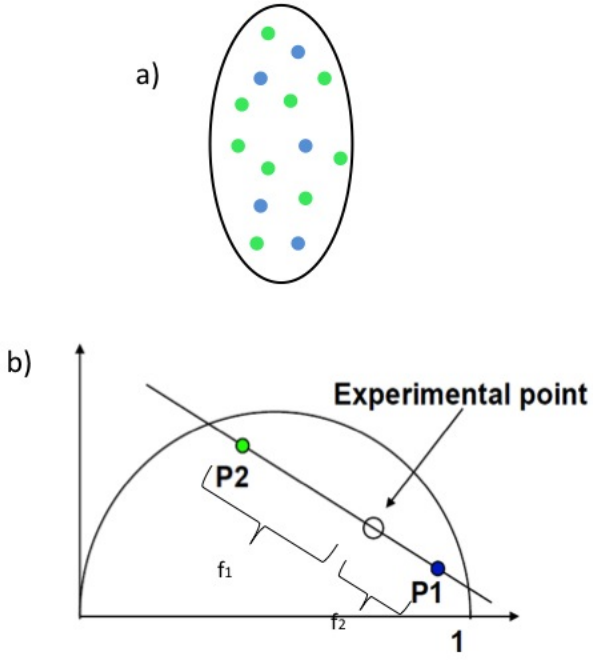

Figure (4.8). *The phasors of two molecular species having multi-exponential decay are located in two specific points in the phasor plot, inside the semicircle. Fig. (a) represents a mixture of green and blue fluorescent species. In Fig. (b), the phasors of all the possible weighting of the two molecular species are located along the straight line connecting the phasors of the two species.*

The phasors of two molecular species having multi-exponential decay are located in two specific points in the phasor plot, inside the semicircle. The phasors of all the possible weighting of the two molecular species are located along the straight line connecting the phasors of the two species. In the case of many molecular species, all the possible combinations are contained in a

polygon where the vertices are coincident with the phasor locations of the different molecular species.

For example, in the case of three molecular species, the possible realizations of the system fill a triangle where the vertices correspond to the phasors of the three pure species. In practice, if the number of molecular species increases, the triangle becomes a polygon with N vertices, where N is the number of molecular species. The N vertices are always the phasors of the N pure species.

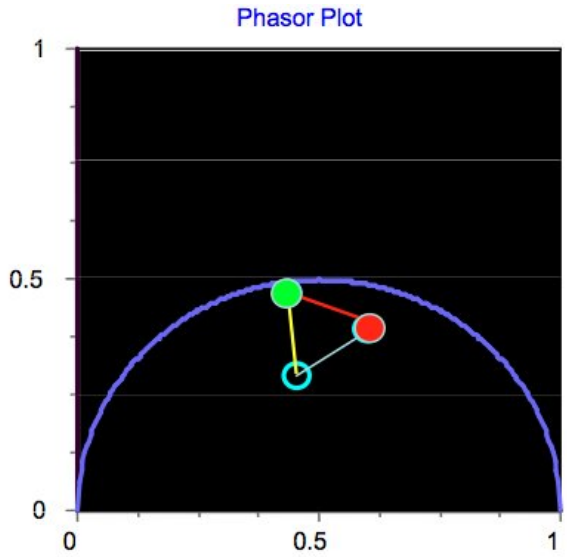

Figure (4.9). *A mixture of N components is bounded by a polygon containing N vertices: in the figure the case of three components is represented. In the Phasor plot, the phasors of three common fluorophores are represented: EGFP (green), autofluorescence (blue) and mRFP1 (red) at 880 nm and two-photon excitation. In any given pixel, mixture of EGFP and autofluorescence must be on the yellow line, mixtures of EGFP and mRFP1 must be on the red line. Mixtures of three of them must be inside the triangle with the corner in the three phasors.*

Every molecular species has a specific location in the phasor plot (phasor fingerprint). However the location in the phasor plot does not correspond biunivocally to one species. Different species can have the same phasor loca-

tion at one frequency even if they have a different lifetime distribution. For example in Fig. 4.10 two species with different lifetime distributions are represented. The red species is a linear combination of lifetimes equal to 3 ns and 0.1 ns, while the blue species is a linear combination of two lifetimes equal to 8 ns and 0.1 ns. The two chemical species have the same position in the phasor plot at the First harmonic. If we represent the same chemical species in a phasor plot at higher frequencies,their location will be separated. For example Fig. 4.11 shows the phasor location at the Second harmonic. There is another fundamental phasor property. Two different molecular species could accidentally have the same lifetime, simply because they can be different combinations of different molecular species that have only the same location in the Phasor Plot. This coincidence happens only for one harmonic. Multi-harmonics analysis separates molecules with two different lifetime distributions and it identifies them univocally. The sensitivity of components separation with higher harmonics analysis is greater for the short lifetime components.

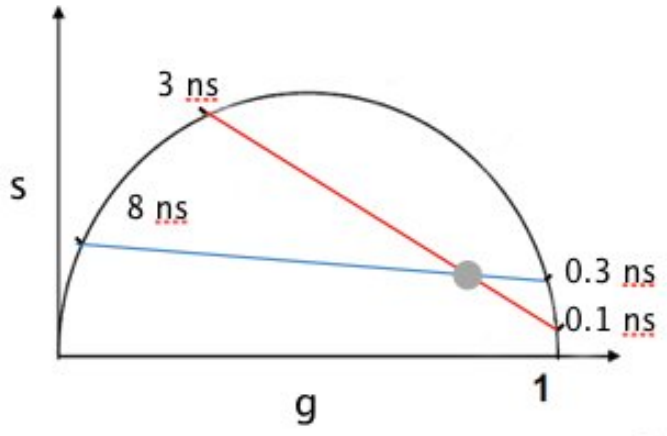

Figure (4.10). *Phasor plot at the First harmonic $\omega = \omega_0$ of two chemical species, ω_0 = 80 MHz. The red species is a linear combination of lifetimes equal to 3 ns and 0.1 ns, while the blue species is a linear combination of two lifetimes equal to 8 ns and 0.1 ns. The two chemical species have the same position in the phasor plot at the 1st harmonic.*

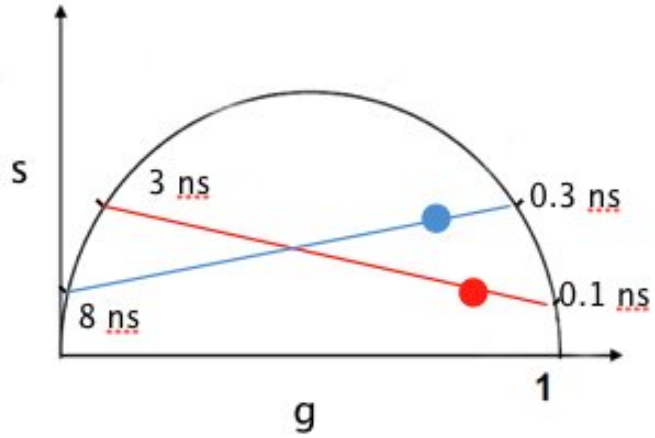

Figure (4.11). *Phasor plot for the Second harmonic $\omega = 2\omega_0$ of the two previous chemical species. At higher frequencies, their location will be separated. For example, the two molecular species have different and separate locations at the Second harmonic. We can observe that the distance of the separated phasors is bigger at lower lifetimes.*

Chapter 5

MATERIALS AND METHODS

5.1 Cell Culture

Federal approved H9 line of hES cells are used. hEs are cultured on a substrate of mouse fibroblast (MEF) feeders (Chemicon Cat PMEF-CF). Plates are first coated with 0.1% - 0.2% gelatin (Sigma G-1393).

MEF feeders are then plated with a density of approximately of 15000 cells per cm^2.

MEF medium: Dulbecco's Modified Eagle Medium (DMEM), 1mM Glutamax (Invitrogen 10569), 10% Fetal Bovine Serum (FBS Invitrogen 16000-044) and 1% non-essential amino acids (Invitrogen 11149-035).

Human Ebrionic Stem (hES) cell medium: DMEM-F12 (Invitrogen 12660), 20% Knokcout serum replacement (KOSR, Invitrogen 10828), 1% non essential amino acids (NEAA, Invitrogen 11140-050), 1mM Glutamax (Invitrogen 35035), 4ug/mL basic fibroblast growthfactors (bFGF, Invitrogen 13256-029) and 0.1 mM beta-mercaptoetanol.

Human Ebrionic Stem (hES) cell are differentiated using bmp4 in the hES medium.

5.2 Immunostaining: Oct4-Immunocytochemistry

Medium is removed from the stem cell plate. Cells are washed with PBS. Cells are fixed in 4% Paraformaldeyde (PF). Cells are washed 3 times with PBS.

Permeabilize with 1 ml cold Methanol for 5 minutes at room temperature. Cells are washed 3 times with PBS. Cells are incubated in blocking buffer with 10% of normal serum in PBS. Serum is from the same species that the secondary antibody: donkey blocking solution at room temperature for 1 hour. The 1st antibody, Goat anti Oct4 is added and cells are incubated for one hour. Cells are washed 3 times.with PBS. The 2nd antibody Inv. Donkey anti-Goat Alexa 568 is addet and celld incubated for one hour. Dapi solution is added to the cell. Finally cells are washed with PBS.

5.3 Imaging

Fluorescence lifetime images were acquired using two-photon microscopy and Immunostaining images were acquired with one photon confocal microscopy.

The first set up is a Zeiss 710 microscope coupled to a Ti: Sapphire laser system (Spectra-Physics Mai Tai) and a ISS A320 FastFLIM [92]. The objective used is a 40 x 1.2 NA water immersion (Zeiss Korr C-Apochromat). The settings for the image acqusition were the following: the image size was 256 x 256 pixels with a scan speed of 25 beginmathendmathm/pixel. In order to separate the fluorescence signal from the laser light and the fluorescence coming from the sample, a dichroic filter with a wavelength of 690 nm has been used. Fluorescence is then detected by a photomultiplier (PMT H7422P-40 of Hamamatsu) and a short pass filter with a wavelength of 610 nm is placed in front of the detector. In fig. 5.1 the set up all the components of the first set up are schematically drawn.

FLIM data were acquired and processed by the SimFCS software developed at the Laboratory of Fluorescence Dynamics. Excitation wavelength of 760 nm was used. The average power used to excite living tissues was about 5 mW. Before proceeding with the experiments, the FLIM calibration of the system was performed by measuring the lifetime of the fluorescein with a single exponential decay and by matching it with a fluorescence lifetime of 4.04 ns. The FLIM data were collected until in the brightest pixel of the image 100 counts were acquired. The acquisition time was typically of the order of few seconds.

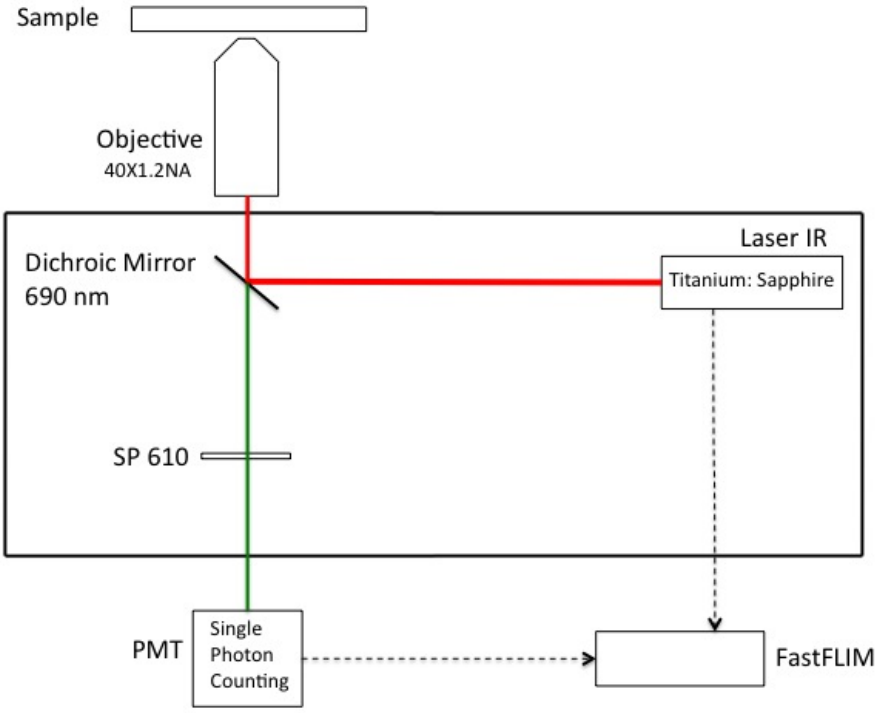

Figure (5.1). *Schematic draw of the experimental setup for FLIM images (Experimental Setup 1). The sample is excited by a infrared laser through two-photon excitation. A dichroic filter (690 nm) separates the fluorescence signal from the laser light and the fluorescence coming from the sample. The photons are collected by a photomultiplier (PMT).*

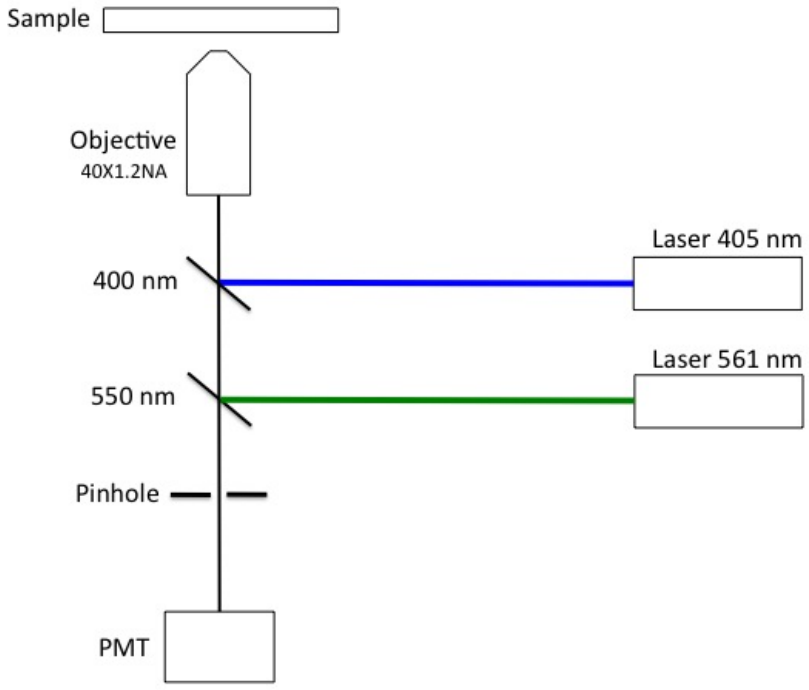

Figure (5.2). *Schematic draw of the experimental setup for immunostaining images (Experimental Setup 2). The images are obtained through two different laser excitations (405 nm and 565 nm), using confocal one-photon laser scanning microscopy.*

5.4 Data Analysis

All phasor transformation and the data analysis of FLIM data are performed using SimFCS software.

Every pixel of the FLIM image is transformed in one pixel in the Phasor Plot. The component g (x-coordinate) and the component s (y-coordinate) of the Phasor Plot are respectively the real and imaginary part of the Fourier transform of the fluorescence intensity response I(t) to the excitation impulse. The data were acquired using the time domain method. The coordinates g and s in the Phasor Plot are calculated from the fluorescence intensity decay of each pixel of the image by using the transformations already defined in Chapter [? 3/4 ?]. The equations are the following:

$$g_{i,j}(\omega) = \frac{\int_0^\infty I_{i,j}(t)\cos(\omega t)dt}{\int_0^\infty I_{i,j}(t)dt} \tag{5.1}$$

$$s_{i,j}(\omega) = \frac{\int_0^\infty I_{i,j}(t)\sin(\omega t)dt}{\int_0^\infty I_{i,j}(t)dt} \tag{5.2}$$

The indices i and j identify the pixel of the image with coordinates i and j. ω is the laser repetition angular frequency ($\omega = 2\pi f$). f is the laser repetition rate, i.e. 80 MHz. All phasor plots are transformed at 80 MHz, i.e. the first harmonic of the laser repetition rate, if not differently specified.

The analysis of the phasor distribution is performed by cluster identification. Clusters of pixel values are detected in specific regions of the Phasor Plot. The cluster assignment is performed by taking in account not only the similar fluorescence properties in the Phasor Plot but also exploiting the spatial distribution and localization in cellular substructures or tissues. We achieve this by applying a median filter that imposes a correlation between cluster of pixels in the Phasor Plot and pixels of the image without decreasing the spatial resolution. This allows better confining a cluster to a specific phasor value, by reducing the statistical error in the phasor associated with each pixel of the image. Regions of the image with different decay profiles and characteristics can be better delineated. In order to obtain information on the chemical composition of tissues, we compare the size of their phasor

distribution with the statistical uncertainty, which depends on the reverse of the square root of the number of photon collected.

$$\sigma \propto \frac{1}{\sqrt{N}} \tag{5.3}$$

If the size of the phasor distribution is comparable to the statistical uncertainty, we select an independent molecular species using a circular selection cursor. If the phasor distribution is elongated, we select a mixture of molecular components using a cursor which joins the two molecular species.

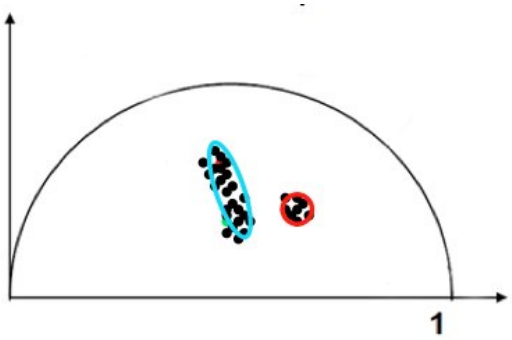

Figure (5.3). *Statistic on the points. Depending on the size of the cluster, it is possible to identify one molecular species or a mixture. If the size of the phasor distribution is comparable to the standard deviation σ, one molecular species is selected using a circular cursor. If σ is elongated, a mixture of of molecular components is selected by a cursor which join the two molecular species.*

Fractional intensities of chemical species (Eq. 4.16 and 4.17) in every pixel of the image are evaluated with a graphical analysis in the phasor plot.

Chapter 6

RESULTS

6.1 Introduction

The phasor approach presented here has the power of drastically simplifying the analysis of FLIM images. Given a FLIM image, the phasor method is able to transform the histogram of the time delay of every pixel in a phasor, an object analogous to a vector. The values of the sine and cosine transforms (Fourier transforms) can be represented in a polar plot, which can be associated to a two-dimensional histogram. In this way, each pixel of the image results in one point in the so-called phasor plot. This identification can also be applied in the reverse mode, each occupied point of the phasor plot can be mapped to a pixel of the image. In other words, since every molecular species has its own specific phasor, the innovative potential of the phasor approach consists of allowing to identify the different molecules exclusively through their position in the phasor plot. Using the phasor approach, all the problems related to the fitting exponential analysis can be avoided and a graphical, easy to understand, global view of the fluorescence decays of the image is immediately provided.

The breakthrough of the phasor approach to FLIM images is that the fluorescence lifetime τ does not need to be calculated anymore. Its knowledge is unnecessary to identify a specific molecular species or to determine the fractional contributions of molecular species at one pixel. If the phasor falls on the "universal circle", it can be unequivocally associated with a lifetime value. If

the phasor is not on the universal circle, the corresponding molecular species must have a complex decay. In this case, estimators of lifetime values can be obtained using phasor plots of higher Fourier harmonics. Concluding, the determination of lifetime components is simply unnecessary when the decay is represented in the phasor plot.

6.2 Results and Discussion

The phasor transformation of FLIM images (described in Chap. 4) of a living tissue directly provides maps of individual tissue components without $a\ priori$ assumption on the number of species present in the tissues [6],[90],[92],[91].

The analysis of a complex system, such as a tissue, results difficult because of all the different molecular species which coexist in the tissue. Applying the phasor approach, each chemical species results to have its specific location in the phasor plot. We are able to determine it through the intrinsic characteristics of the fluorescence decay and this characteristic "phasor fingerprint" allows us to identify individual components in a tissue. Fig. 6.1 shows the location in the phasor plot of the most important fluorophores. Their positions in the plot are well defined and clearly separated one from the other.

The majority of fluorophores have decay with multiple exponential components because of their conformational heterogeneity.

The phasor position of pure GFP is near, but not exactly, on the universal circle, since the fluorescence decay of GFP is not single exponential [93]. Collagen has a very short lifetime with a broad distribution of decay components due to intermolecular cross links [94]. Its phasor is located inside the universal circle, close to the temporal zero. The phasor position of retinol in DMSO has a specific location which is different from the one of retinoic acid in DMSO, in agreement with the measured multiexponential decays in ref [95]. Both FAD and free and bound NADH phasor position are located inside the phasor plot. Their lifetime is a combination of several exponential components [96],[97]. The phasor position of protoporphyrin IX (in dimethylformamide and methanol) is located on the universal circle since it is characterized by a single lifetime component [98].

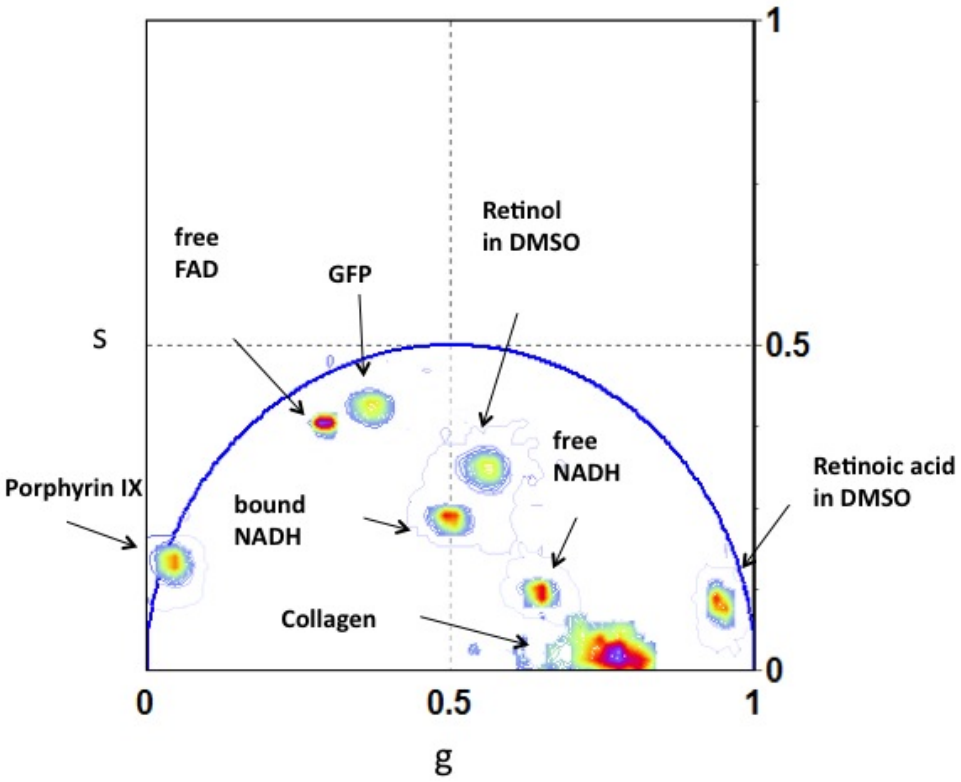

Figure (6.1). *"Phasor fingerprint" of pure chemical species: phasors of pure chemical species identify tissue components through their location in the Phasor Plot. In the figure the location of the following chemical species are represented: GFP in Tris buffer, Retinol in DMSO (pH 8.5), Retinoic acid in DMSO (pH 8.5), FAD in water (pH 7), free NADH in Mops buffer (pH 7), bound NADH in in Mops buffer 1:1 with lactate dehydrogenase (pH 7), Protoporphyrin IX in dimethylformamide: methanol (pH 7).*

The phasor position can be obtained from published lifetime decay data after application of the phasor transformation. We emphasize that in the phasor approach the peculiarity that characterizes a specific tissue component is the location in the phasor plot.

The phasor location of endogenous fluorophores is used as a guide to identify them in living tissues. This map will be used for the analysis of the following data.

The analysis of the FLIM data in the phasor space is performed by detecting clusters of pixel values in specific regions of the phasor plot. Fig. 6.2 (A) displays two-photon excited fluorescence image of undifferentiated hES. The phasor analysis of the FLIM was performed by a mathematical transformation of the raw data as explained in Chap. 5. Fig. 6.2 (B) displays the two-dimensional phasor plot of the FLIM image. Every pixel of the FLIM image is transformed into a pixel in the phasor plot. All the pixels are located inside the universal circle of the phasor plot, thus indicating that their decay is multi-exponential. The phasor distribution of the the living tissue has a complex shape with different clusters. Their positions specifically correspond to different chemical components.

In Fig. 6.2 (C) pixels are highlighted with a color that corresponds to the clusters in the phasor plot (red, green and blue clusters). The red colored cluster selects specific bright granules, which results to contain porphyrin. This deduction can be done observing Fig. 6.1. The phasor location of the molecular species in Fig. 6.1 is used as a reference to analyze the phasor distribution in Fig. 6.2. The red cluster is located in the position of the phasor which is very close to the Porphyrin IX in the phasor plot in Fig. 6.1. Observing the position in the phasor plot, Porphyrin has a very long fluorescence lifetime. The green cluster selects the hES colony. Finally, the blue cluster selects an area which is located outside the hES colony. It selects autofluorescence of MEFs which is positioned in the central zone of the phasor plot, typical of autofluorescence of somatic cells. The autofluorescence is located in the middle of the phasor plot because it is a mixture of many intrinsic fluorescence, such as NADH.

The histogram of the τ_ϕ values is represented in Fig. 6.2 (D), colored in grey. The colored clusters are also highlighted in the histogram. τ_ϕ values are

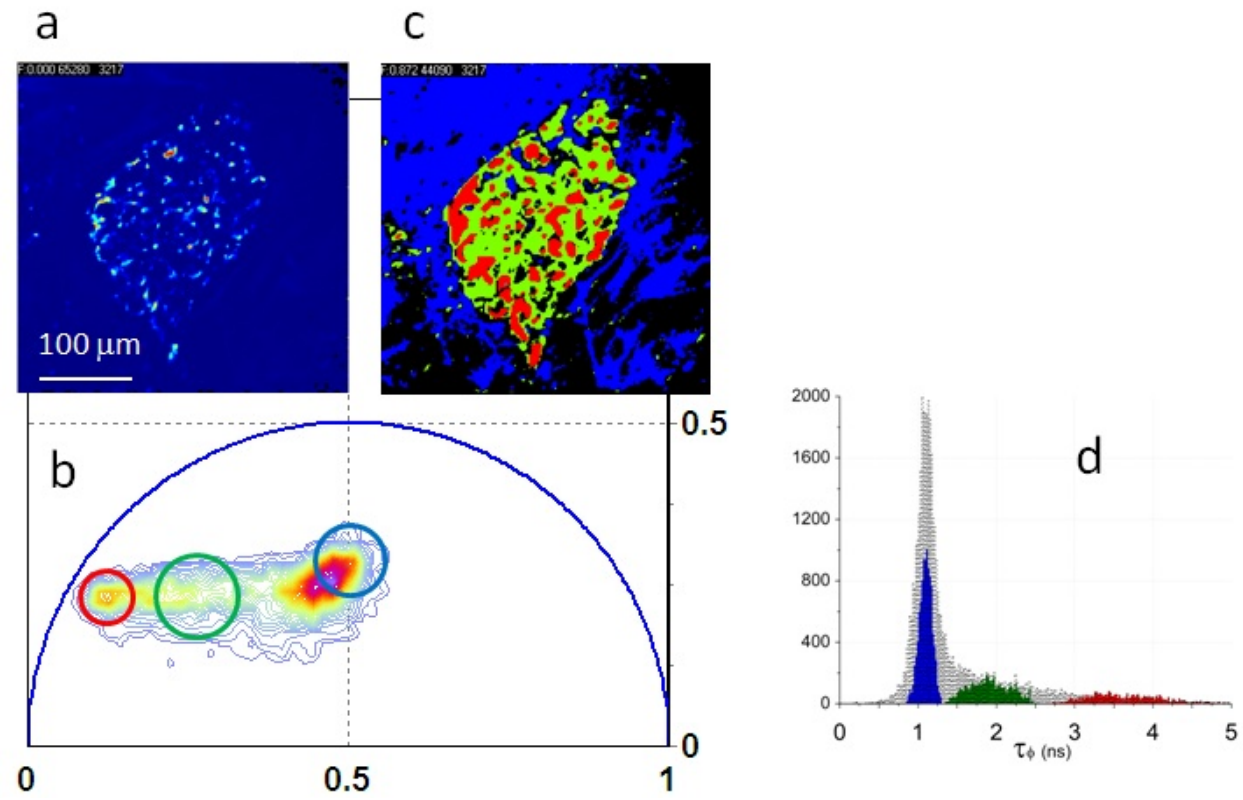

Figure (6.2). *Phasor analysis of FLIM tissue images separates tissue components. (A) Intensity image of undifferentiated hES. (B) Phasor plot of the FLIM image. Three clusters corresponding to different tissue components are identified in the phasor distribution with different colors. (C) Phasor color maps of the FLIM image. The colors of pixels correspond to the clusters of tissue components identified in the phasor plot. (D) Average lifetime τ_ϕ histograms of the FLIM image is represented in grey. The colored areas correspond to the τ_ϕ of each tissue component identified by the phasor analysis.*

calculated using Eq. 3.13. The fluorescence lifetime differences can be easily discriminated in the phasor plot, while it is difficult to discriminate them in the lifetime histogram. The lifetime τ_ϕ has a range from 0.5 to 4.5 ns, it shows a high peak at about 1 ns, after which the distribution decreases slowly until 4.5 ns. Observing the three lifetimes of the colored clusters, they can be easily discriminated and each of them has its specific value.

Hence, phasor approach is a "fit-free" method that requires no assumption or a priori knowledge on the biological sample, such as its biochemical content. Tissue components are are identified and separated by cluster analysis , i.e. detecting clusters of pixel values in specific regions in the phasor plot. This method provides high selectivity in identifying fluorescence components that cannot be separated by a multi-exponential fitting or by analyzing the average lifetime. Multi-exponential fitting can separate only a limited number of components in a mixture of multiple fluorescent species. The mean lifetime offers a contrast whose physical interpretation is ambiguous and cannot separate tissue components with the same average lifetime but characterized by different lifetime distributions. Instead, the phasor approach provides excellent discrimination of intrinsic molecular sources in live tissues, where the majority of pixels have a complex multi-exponential decay.

6.3 hES and Immunostaining

The hallmark of stem cells is their self-renewal ability. A stem cell can produce either daughters which maintain stem-cell identity, and therefore remain in an undifferentiated state, either differentiating daughters which are committed to form specialized tissues [7]. In particular, pluripotent stem cells can give rise to all cell types in a given organ. Furthermore, through different matrices and stimulation factors, pluripotent hES cells can be induced to differentiate into blood cells, muscle cells and nerve cells.

Recognizing the differentiation state of stem cell is an extremely informative and useful task. Several advantages may derive from this knowledge, for example it would be helpful to better comprehend the factors which can induce a differentiation toward a certain type of cell instead of another. The three most common markers for pluripotency are Oct4 [7], NANOG [99] and

SOX2 [100].

Oct4 is a transcription factor which governs ES pluripotency [101]. Oct4 has a critical role in the establishment and maintenance of pluripotent state. Differentiation of pluripotent cells is associated with downregulation of Oct4 levels, and downregulation of the Oct4 gene in ES cells results in the differentiation and loss of pluripotent cells [102][103].

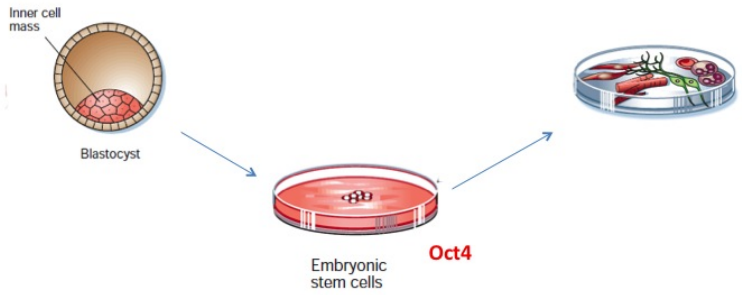

Figure (6.3). *Identifying human Embryonic Stem cells (hES) in vitro. The H9 line was used. Through different matrices and stimulation factors, hES cells can be induced to differentiate into blood cells, muscle cells and nerve cells etc. Oct4 is a marker for pluripotent stem cells and its downregulation results in the differentiation and loss of pluripotent cells [7].*

Fig. 6.4 represents different images of an undifferentiated pluripotent hES colony. The fluorescence intensity image is represented in Fig. 6.4 (A), Fig. 6.4 (C) is the phasor color map obtained through the cluster analysis of Fig. 6.4 (B). The colony os stem cells is clearly highlighted by green and red pixels, which correspond to porphyrin (red cluster) and to a chemical species (green cluster) which appears to be a linear combination of porphyrin and MEF (blue cluster in the central zone of the phasor plot). Hence, using the

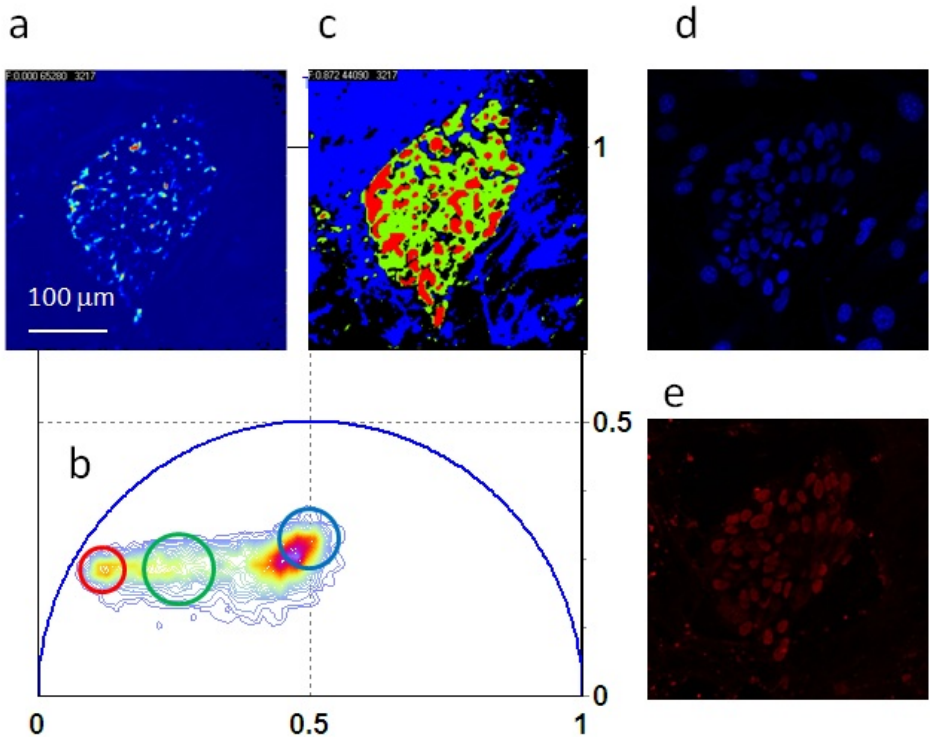

Figure (6.4). *Maps of relative concentration of tissue components in undifferentiated pluripotent hES. (A) Intensity image of undifferentiated hES. (B) Phasor plot of the FLIM image. Different clusters are assigned to pure chemical species according to Fig. 6.5: porphyrin granules (1) in red, hES colony (2) in green, MEF cytoplasm (3) in blue. (C) Phasor color map. Pixels of different colors correspond to the color of the cluster in the phasor plot. Red pixels contain mostly porphyrin, green pixels highlight the hES colony and blue pixels identify MEFs. (D) Image with DAPI. DAPI is a standard marker, able to label the nucleus of the cells. (E) Image of the colony after immunostaining. Immunostaining was done labeling the transcription factor Oct4 with antibodies through Alexa Fluor 568. Oct4 is a specific marker of pluripotent stem cells.*

phasor approach to FLIM images we are able to identify the undifferentiated stem cells colony only through the cluster analysis, without having any a priori information. The hES colony is noticeable identifyed by the red and the green cluster.

After in vivo measurements with FLIM, we fixed the cells. In order to identify stem cells colonies, we treated the stem cells colony to perform immunostaining procedure. After fixation and immunostaining the cells are unviable and unrecoverable, they become incompatible with $in\ vivo$ dynamic observations. However, immunostaining gives us reliable information about cells and it allows us to identify stem cells and fibroblats. It is a standard procedure, validated and currently used.

Fig. 6.4 (D) illustrates the results after fixation through DAPI. DAPI or 4',6-diamidino-2-phenylindole is a fluorescent stain that binds strongly to DNA. It is used extensively in fluorescence microscopy. DAPI is able to pass through an intact cell membrane and though it is used to stain both live and fixed cells, but in fixed cells the procedure is relevantly more efficient and it gives better results. DAPI binds to the chromatin of the nucleus and though it identifyes the nuclei of cells. It is not a specific dyes of stem cells. So, using DAPI, we can observe all the nuclei of cells, either stem cells and ME fibroblasts. We can clearly identify the stem cells colony. It corresponds to the colony which we identified previously through the phasor cluster analysis of the FLIM image.

Fig. 6.4 (E) illustrates immunostaining results of Oct4 linked with Alexa Fluor 568 (see Cell Colture and Immunostaining, Chap. 5.1). As I mentioned before, Oct4 is a specific marker of stem cells pluripotency. By visualizing the expression of Oct4, linked with antibodies through Alexa Fluor 568, we can identify stem cells and measure their state of differentiation. It is able not only to identify stem cells, but more specifically to identify undifferentiated stem cells. The efficiency of the immunostaining is as higher as the stem cells are not differentiating in specialized tissues. Indeed, this type of immunostaining is extremely informative for analysis and measurement of stem cells differentiation. The main disadvantage is that after the fixation stem cells cannot be monitored $in\ vivo$ anymore and they become unviable for further analysis. Observing Fig. 6.4 (E), the hES colonies express Oct4-Alexa Fluor

568. Instead, since Oct4 is a specific marker of stem cells, it is not expressed in nuclei of MEFs. The stem cells colony (in red) corresponds exactly to the colony we had previously highlighted through phasor cluster analysis of the FLIM image in Fig. 6.4 (C).

Through DAPI fixation and Oct4-Alexa Fluor 568 immunostaining, we were able to confirm the validity of the analysis performed in FLIM images by the phasor approach. The red and the green cluster can efficiently identify the hES colony. This method does not require to fix the cells, it is not invasive at all and it is very fast. Stem cells remain viable for further analysis and they can be monitored *in vivo*.

6.4 Undifferentiated and Differentiating Stem Cells

We firstly obtained FLIM images in vivo, using two-photon laser. Then we applied fixation and immunostaining procedures to identify stem cell colonies and we acquired the images with a one-photon confocal laser.

We performed the same procedures in both undifferentiated and differentiating stem cells.

Hence, we obtained the FLIM image, the image after fixation with DAPI and the image after immunostaining with Oct4-Alexa Fluor 568 of a differentiating hES colony. Our goal is comparing the results given by the undifferentiated and the differentiated colony, in order to understand whether the phasor cluster analysis of FLIM image is able to discrimate them. In other words, we want to verify if the phasor approach can be a valide and effective tool to measure stem cell differentiation. Moreover, we want to understand if we can obtain further information about the chemical species prevalent in undifferentiated or differentiating stem cells.

The first row of Fig. 6.5 (A) consists of a brightfield image (transmission image), a FLIM image and a phasor map of the FLIM image of undifferentiated hES. The same images are represented in the second row, but this time they belong to differentiating hES. The brightfield image is only a visualization image, while the FLIM image is the one used for our analysis. FLIM measurement is independent from the absolute concentration of a fluorescent species but reveals the relative concentration of two or more fluorophores

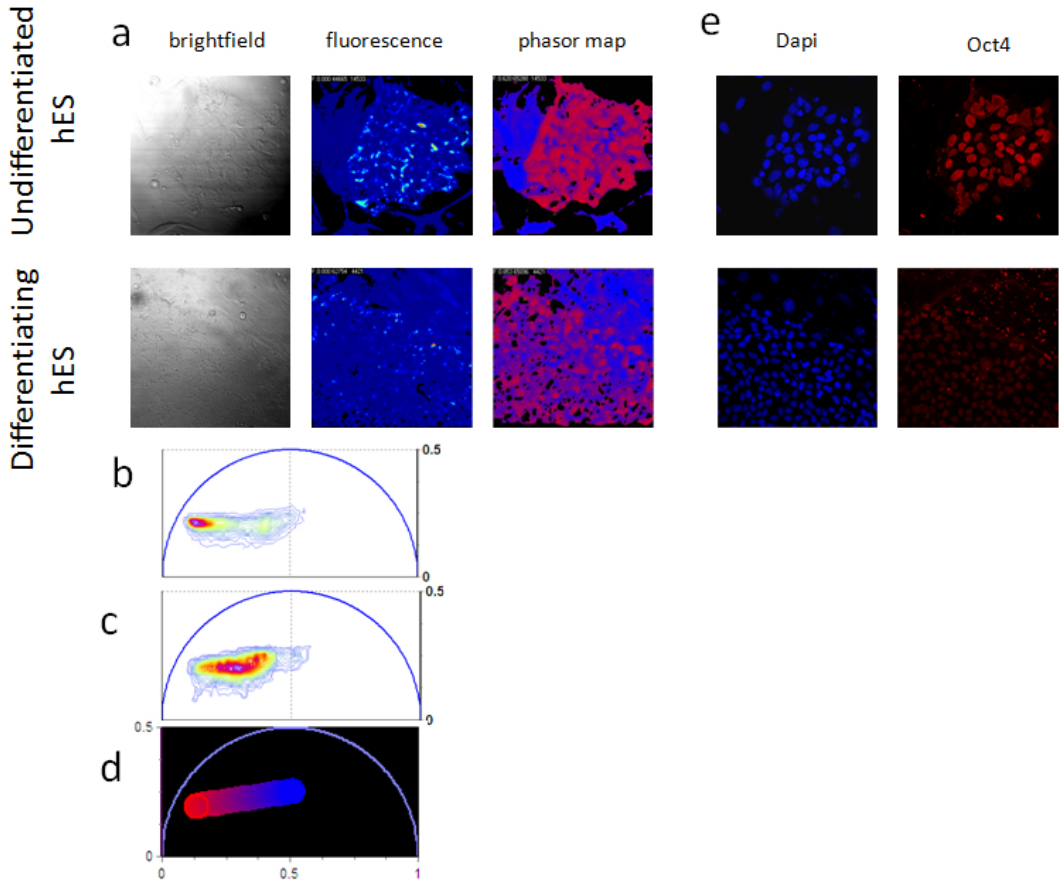

Figure (6.5). *Comparison between undifferentiated and differentiating hES. (A) Brightfield, FLIM, phasor map of the FLIM images of undifferentiated hES (pluripotent) and differentiating hES (treated with Bmp4). (B) Phasor plot of the FLIM image of undifferentiated hES. (C) Phasor plot of the FLIM image of differentiating hES. (D) Phasor plot selection using linear clusters that represent all the possible relative concentrations of porphyrin and MEFs autofluorescence. Each point along the line has a color corresponding to specific fractional intensity of the species. (E) Images of the undifferentiated and differentiating colony after immunostaining with DAPI and with Oct4.*

weighted by their intensity. This property allows us to map the relative concentration of intrinsic fluorophores. In the phasor plot a combination of two chemical species lie on the line connecting the two phasors (as explained in Chap. 4 and 5).

Fig. 6.5 (B) and (C) represent the phasor plot respectively of the undifferentiated hES image and the differentiating hES image. The phasor position of the bright granules which are identified by the red cluster co-localize with the porphyrin in the phasor plot of pure chemical species (Fig. 6.1). The average autofluorescence arising from the tissue (blue cluster) locates in the central part of the phasor plot. We recall that this is because it is a mixture of different intrinsic fluorescent components and we associated it to MEFs autofluorescence.

The phasors originated by the fluorescence stem cells signal are located along the straight line which joins the position of porphyrin and MEFs autofluorescence. We provided a phasor map of the relative concentration of the two components within the tissues by visualizing their fractional intensities to the signal. The relative concentration is calculated in every pixel of the image with a graphical analysis, by the position of the pixel in the phasor plot along the line connecting the two molecular species.

In Fig. 6.5 (D), the linear cluster with the color scale from red to blue shows all the possible relative concentrations of porphyrin and autofluorescence. Each point along the cluster has a color corresponding to the specific fractional intensity. The same color scale is used to map the relative concentration of the two species in the phasor map of Fig. 6.5 (A). The phasor position of cells with different expression of porphyrin lie along the line between the porphyrin and the autofluorescence phasor points. Using this principle, we directly visualized different state of differentiation of the hES within the tissue.

Observing the phasor maps of Fig. 6.5 (A), we notice immediately that the two images differ. The phasor map of the undifferentiated hES colony has prevalently red pixels. This means that undifferentiated stem cells express a high concentration of porphyrin granules. Instead, the color of the pixels of differentiating stem cells is not only red but it tends to the blue cluster. This means that the relative concentration of the chemical species is different. We

identified different concentrations of porphyrin and we can relate this different concentration to different states of differentiation of stem cells. While the stem cells are differentiating, the phasor position moves from the porphyrin to MEFs autofluorescence. The more stem cells are differentiating, the lower becomes the relative concentration of porphyrin. In the literature we can find that porphyrins are involved in colony expansion and in the pathway of self-renewal of hES [104].

In order to confirm our results, we performed again fixation with DAPI and immunostaining with Oct4 linked through Alexa Fluor 568. We can observe the corrispondent images in Fig. 6.5 (E). The fixation with DAPI is not very informative, DAPI simply stains the nuclei of stem cells. Instead, the immunostaining with Oct4-Alexa Fluor 568 allows us to measure the state of differentiation of hES. By looking at the fluorescence intensity, we can measure the expression of Oct4 in stem cells. Undifferentiated hES have an high expression Oct4, the image is extremely bright. Differentiating hES have a lower expression of Oct4. The correspondent image is indeed not as bright as previously and this indicates a loss of pluripotency.

The images obtained with Oct4 immunostaining gave us the same information of the images obtained with the phasor color map of FLIM images. Using Oct4-Alexa Fluor 568 immunostaining, we can see the expression of Oct4 decreasing while the hES are differentiating and loosing their pluripotency. The change we can observe in the FLIM images is associated to cells differentiation. Using the phasor approach to analyze the FLIM image, we can measure the state of differentation of stem cells looking at their phasor position. The more the phasor moves along the red-blue linear cluster, the more hES are differentiating. Through the phasor approach we are able to individualize the chemical species which are present in stem cells living tissues and which change during differentiation.

Chapter 7

CONCLUSIONS

Time lapse phasor FLIM imaging can be used to achieve information on dynamic of cell activities, physiological processes thus monitoring tissue development over time. FLIM was already been performed to distinguish between different states of stem cells in vitro. However, our approach was particularly non invasive.

We performed FLIM measurements without any extrinsic labeling, only using intrinsic fluorophores present in the cells. The FLIM images were acquired in vivo. After the measurements, we analyzed the images without any a priori assumption through the phasor approach.

The phasor approach to FLIM gives a straightforward and quantitative interpretation of physiological processes which occur in living cells. This method is able to simultaneously identify chemical components, it allows fast analysis of wide data sets and it offers a global view of the decay properties by analyzing all pixels of the image at the same time.

Phasors allow an easy quantification of the relative concentration of molecular species in vivo. The phasor location of some relevant endogenous fluorophores, such as collagen, NADH, FAD, porphyrin, retinol and retinoic acid were determined. For some of these metabolic products direct labeling is not possible. However, the number of fluorescent chemical species that can be identified by their phasor signature is not limited. The phasor location of every molecular species in the plot is uniquely determined by its fluorescence decay. The "phasor fingerprint" of chemical species reduces the importance

of knowing the exact lifetime distribution of fluorophores decay and allows interpreting FLIM images directly in terms of chemical species.

Phasor coordinates are a linear function of molecular species and mixture of fluorescent species can be identified by a graphical analysis. We were able to measure the relative concentration of fluorescent species directly from the position of the pixel in the phasor plot along the straight line connecting two chemical species. We quantified different relative concentrations of endogenous fluorophores in undifferentiated and differentiating stem cells. This provides important information about the distribution of porphyrin and MEFs autofluorescence within the stem cells. By using the phasor approach to FLIM, we were able to distinguish between undifferentiated and differentiating stem cells observing the phasor position. The phasor location gives us important information about the chemical species which are present in stem cells tissues. We can measure which chemical species are prevalent in undifferentiated or differentiating stem cells and which chemical changes occur while the stem cells are differentiating.

We demonstrated that the phasor approach in living cells results to be a promising tool in biomedical research, biology and biophotonics. It allows to track *in vivo* metabolic changes which carry information about stem cell differentiation but can also be associated to cell carcinogenesis, apoptosis and necrosis. The ability to observe noninvasively the chemical species prevalent within stem cells tissue and their relation to the differentiation state could be extremely useful. Label-free discrimination between self-renewal and differentiation by phasor approach to FLIM is suitable to monitor embryonic stem cells fate. Furthermore, mapping the relative concentrations of chemical species may be extremely helpful to identificate specific intrinsic biomarkers which bring stem cells to differentiate into various lineages.

In the field of tissue engineering, we want to distinguish between undifferentiated and differentiating stem cells in the less invasive way possible. The recent and promising studies of induced Pluripotent Stem cells require to select and sort undifferentiated and differentiating stem cells. We demonstrated that the phasor approach to FLIM can be a suitable and optimum tool for label-free *cell sorting* in vivo and in real time.

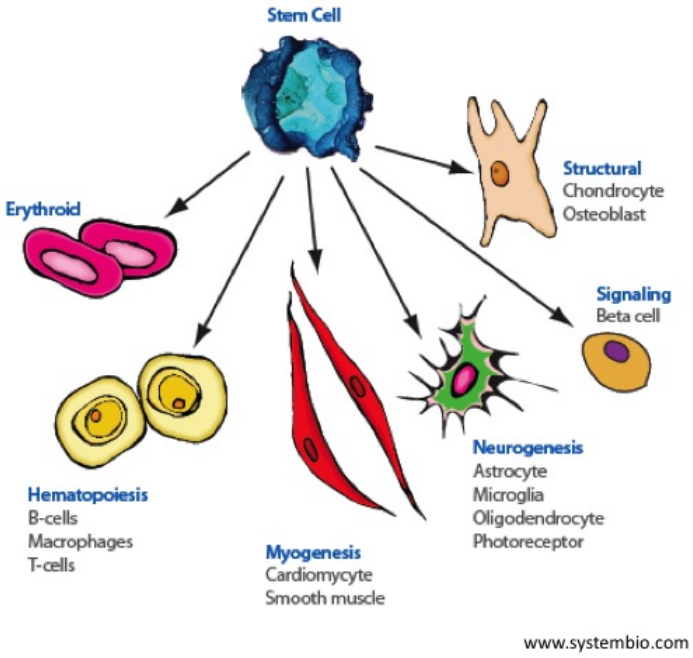

Figure (7.1). *Future perspectives of cell sorting. One of the possible future direction can be identifying the appropriate intrinsic biomarkers to monitor and trace differentiation of stem cells in different progenies.*

Grazie

Credo che l'anno appena passato sia stato il piú forte della mia vita. Per molti motivi. E per tutto l'anno questa tesi mi é stata accanto, mi ha accompagnato, mi ha entusiasmato, mi ha riempito le giornate. Posso dire che in alcuni giorni mi ha addirittura aiutato.

Ci sono innanzitutto tre persone che devo ringraziare per averla resa possibile: il mio meraviglioso advisor a UC Irvine Enrico Gratton, Chiara Stringari che mi ha seguito passo passo con infinita pazienza e il prof. Alfredo Ruggeri, sempre disponibile ad assistere e consigliare quella pazza ragazza oltreoceano. Senza di loro non sarei da nessuna parte.

Moltissimi altri mi sono stati vicini in quest'anno e ciascuno a modo suo mi ha dato ogni giorno un po' di forza. La mia famiglia, ristretta e allargata, che é la famiglia piú bella e unita che io abbia mai incontrato. Tutti i miei amici, italiani e "americani"; sono stata davvero fortunata ad avere accanto persone cosí speciali.

Ci saranno tante persone accanto a me quando presenteró questo bellissimo progetto, prima fra tutte mia madre. E purtroppo ci sará una grande assenza, che non avevo mai previsto. Proprio lui che ha voluto tutto questo per me, che mi regalato tutto questo. A volte non so cosa darei per poterlo riavere indietro. Ma oggi sono qui, e sono qui grazie a lui. E allora mi fermeró, e penseró ai suoi occhi buoni e al suo sorriso, e lo sentiró. Ripeteró sottovoce, tra me e me, "Accidenti, Ottavia" e lui ci sará. So che questa giornata non puó proprio perdersela. Grazie.

Bibliography

[1] Martin F Pera and Patrick P L Tam. Extrinsic regulation of pluripotent stem cells. *Nature*, 465(7299):713–20, Jun 2010.

[2] J A Thomson, J Itskovitz-Eldor, S S Shapiro, M A Waknitz, J J Swiergiel, V S Marshall, and J M Jones. Embryonic stem cell lines derived from human blastocysts. *Science*, 282(5391):1145–7, Nov 1998.

[3] B E Reubinoff, M F Pera, C Y Fong, A Trounson, and A Bongso. Embryonic stem cell lines from human blastocysts: somatic differentiation in vitro. *Nat Biotechnol*, 18(4):399–404, Apr 2000.

[4] Kazutoshi Takahashi and Shinya Yamanaka. Induction of pluripotent stem cells from mouse embryonic and adult fibroblast cultures by defined factors. *Cell*, 126(4):663–76, Aug 2006.

[5] Kazutoshi Takahashi, Koji Tanabe, Mari Ohnuki, Megumi Narita, Tomoko Ichisaka, Kiichiro Tomoda, and Shinya Yamanaka. Induction of pluripotent stem cells from adult human fibroblasts by defined factors. *Cell*, 131(5):861–72, Nov 2007.

[6] DM JAMESON, E GRATTON, and RD HALL. The measurement and analysis of heterogeneous emissions by multifrequency phase and modulation fluorometry. *Applied Spectroscopy Reviews*, 20(1):55–106, 1984.

[7] P J Donovan and J Gearhart. The end of the beginning for pluripotent stem cells. *Nature*, 414(6859):92–7, Nov 2001.

[8] Sreelaja Nair and Thomas F Schilling. Chemokine signaling controls endodermal migration during zebrafish gastrulation. *Science*, 322(5898):89–92, Oct 2008.

[9] Elaine Fuchs. Skin stem cells: rising to the surface. *J Cell Biol*, 180(2):273–84, Jan 2008.

[10] Yanfeng Lin, Mark E Gill, Jana Koubova, and David C Page. Germ cell-intrinsic and -extrinsic factors govern meiotic initiation in mouse embryos. *Science*, 322(5908):1685–7, Dec 2008.

[11] David T Scadden. The stem-cell niche as an entity of action. *Nature*, 441(7097):1075–9, Jun 2006.

[12] A Spradling, D Drummond-Barbosa, and T Kai. Stem cells find their niche. *Nature*, 414(6859):98–104, Nov 2001.

[13] Elaine Dzierzak and Tariq Enver. Stem cell researchers find their niche. *Development*, 135(9):1569–73, May 2008.

[14] Karolina Archacka, Iwona Grabowska, and Maria A. Ciemerych. Induced pluripotent stem cells - hopes, fears and visions. *Postepy Biologii Komorki*, 37(1):41–62, 2010.

[15] Han-Wen Guo, Chien-Tsun Chen, Yau-Huei Wei, Oscar K Lee, Vladimir Gukassyan, Fu-Jen Kao, and Hsing-Wen Wang. Reduced nicotinamide adenine dinucleotide fluorescence lifetime separates human mesenchymal stem cells from differentiated progenies. *J Biomed Opt*, 13(5):050505, 2008.

[16] Sven R Kantelhardt, Jan Leppert, Jochen Krajewski, Nadine Petkus, Erich Reusche, Volker M Tronnier, Gereon Hüttmann, and Alf Giese. Imaging of brain and brain tumor specimens by time-resolved multiphoton excitation microscopy ex vivo. *Neuro Oncol*, 9(2):103–12, Apr 2007.

[17] KA Kasischke, HD Vishwasrao, PJ Fisher, WR Zipfel, and WW Webb. Neural activity triggers neuronal oxidative metabolism followed by astrocytic glycolysis. *Science*, 305(5680):99–103, July 2004.

[18] William L Rice, David L Kaplan, and Irene Georgakoudi. Two-photon microscopy for non-invasive, quantitative monitoring of stem cell differentiation. *PLoS One*, 5(4):e10075, 2010.

[19] Melissa C Skala, Kristin M Riching, Annette Gendron-Fitzpatrick, Jens Eickhoff, Kevin W Eliceiri, John G White, and Nirmala Ramanujam. In vivo multiphoton microscopy of nadh and fad redox states, fluorescence lifetimes, and cellular morphology in precancerous epithelia. *Proc Natl Acad Sci U S A*, 104(49):19494–9, Dec 2007.

[20] Aisada Uchugonova and Karsten König. Two-photon autofluorescence and second-harmonic imaging of adult stem cells. *J Biomed Opt*, 13(5):054068, 2008.

[21] Fritjof Helmchen and Winfried Denk. Deep tissue two-photon microscopy. *Nat Methods*, 2(12):932–40, Dec 2005.

[22] JR ALCALA, E GRATTON, and FG PRENDERGAST. Fluorescence lifetime distributions in proteins. *Biophysical Journal*, 51(4):597–604, April 1987.

[23] Claire N Medine, Angela McDonald, Axel Bergmann, and Rory R Duncan. Time-correlated single photon counting flim: some considerations for physiologists. *Microsc Res Tech*, 70(5):420–5, May 2007.

[24] I Gryczynski, H Szmacinski, and J R Lakowicz. On the possibility of calcium imaging using indo-1 with three-photon excitation. *Photochem Photobiol*, 62(4):804–8, Oct 1995.

[25] JR Lakowicz, I Gryczynski, H Malak, M Schrader, P Engelhardt, H Kano, and SW Hell. Time-resolved fluorescence spectroscopy and imaging of dna labeled with dapi and hoechst 33342 using three-photon excitation. *Biophysical Journal*, 72(2):567–578, February 1997.

[26] S Maiti, J B Shear, R M Williams, W R Zipfel, and W W Webb. Measuring serotonin distribution in live cells with three-photon excitation. *Science*, 275(5299):530–2, Jan 1997.

[27] RM Williams, JB Shear, WR Zipfel, S Maiti, and WW Webb. Mucosal mast cell secretion processes imaged using three-photon microscopy of 5-hydroxytryptamine autofluorescence. *Biophysical Journal*, 76(4):1835–1846, April 1999.

[28] C Xu, W Zipfel, JB Shear, RM Williams, and WW Webb. Multiphoton fluorescence excitation: New spectral windows for biological nonlinear microscopy. *Proceedings of the National Academy of Sciences of the United States of America*, 93(20):10763–10768, October 1996.

[29] WR Zipfel, RM Williams, R Christie, AY Nikitin, BT Hyman, and WW Webb. Live tissue intrinsic emission microscopy using multiphoton-excited native fluorescence and second harmonic generation. *Proceedings of the National Academy of Sciences of the United States of America*, 100(12):7075–7080, June 2003.

[30] I FREUND and M DEUTSCH. 2nd-harmonic microscopy of biological tissue. *Optics Letters*, 11(2):94–96, February 1986.

[31] PJ Campagnola and LM Loew. Second-harmonic imaging microscopy for visualizing biomolecular arrays in cells, tissues and organisms. *Nature Biotechnology*, 21(11):1356–1360, November 2003.

[32] PJ Campagnola, AC Millard, M Terasaki, PE Hoppe, CJ Malone, and WA Mohler. Three-dimensional high-resolution second-harmonic generation imaging of endogenous structural proteins in biological tissues. *Biophysical Journal*, 82(1):493–508, January 2002.

[33] Y Barad, H Eisenberg, M Horowitz, and Y Silberberg. Nonlinear scanning laser microscopy by third harmonic generation. *Applied Physics Letters*, 70(8):922–924, February 1997.

[34] M Muller, J Squier, KR Wilson, and GJ Brakenhoff. 3d microscopy of transparent objects using third-harmonic generation. *Journal of Microscopy-Oxford*, 191:266–274, September 1998.

[35] M. Goppert-Mayer. Uber elementarekte mit zwei quantensprunger. *Ann. Phys.*, 9(273), 1931.

[36] Warren R Zipfel, Rebecca M Williams, and Watt W Webb. Nonlinear magic: multiphoton microscopy in the biosciences. *Nat Biotechnol*, 21(11):1369–77, Nov 2003.

[37] Axel Bergmann Wolfgang Becker. *Lifetime Imaging Techniques for Optical Microscopy*, 2003.

[38] C. Xu and W.W. Webb. Xu, c. and webb, w.w. *Topics in Fluorescence Spectroscopy: Nonlinear and Two-Photon-Induced Fluorescence*, 5:471–540, 1997.

[39] C. Xu and W.W. Webb. Measurement of two-photon excitation cross sections of molecular fluorophores with data from 690 nm to 1050 nm. *J. Opt. Soc.Am. B*, 13:481–491, 1996.

[40] Masters B.R. Webb W.W. Piston, D.W. Three-dimensionally resolved nad(p)h cellular metabolic redox imaging of the in situ cornea with two-photon excitation laser scanning microscopy. *J. Microsc.*, (178 (Pt 1)):20–27, 1995.

[41] Daniel R Larson, Warren R Zipfel, Rebecca M Williams, Stephen W Clark, Marcel P Bruchez, Frank W Wise, and Watt W Webb. Water-soluble quantum dots for multiphoton fluorescence imaging in vivo. *Science*, 300(5624):1434–6, May 2003.

[42] M Albota, D Beljonne, J L Brédas, J E Ehrlich, J Y Fu, A A Heikal, S E Hess, T Kogej, M D Levin, S R Marder, D McCord-Maughon, J W Perry, H Röckel, M Rumi, G Subramaniam, W W Webb, X L Wu, and C Xu. Design of organic molecules with large two-photon absorption cross sections. *Science*, 281(5383):1653–6, Sep 1998.

[43] X Zhou, AM Ren, JK Feng, XJ Liu, JX Zhang, and JZ Liu. One- and two-photon absorption properties of novel multi-branched molecules. *Physical Chemistry Chemical Physics*, 4(18):4346–4352, 2002.

[44] W Wang, JB Wyckoff, VC Frohlich, Y Oleynikov, S Huttelmaier, J Zavadil, L Cermak, EP Bottinger, RH Singer, JG White, JE Segall, and JS Condeelis. Single cell behavior in metastatic primary mammary tumors correlated with gene expression patterns revealed by molecular profiling (vol 62, pg 6278, 2002). *Cancer Research*, 62(23):7132–7132, December 2002.

[45] ZF Mainen, M Maletic-Savatic, SH Shi, Y Hayashi, R Malinow, and K Svoboda. Two-photon imaging in living brain slices. *Methods-A Companion To Methods In Enzymology*, 18(2):231–+, June 1999.

[46] SH Shi, Y Hayashi, RS Petralia, SH Zaman, RJ Wenthold, K Svoboda, and R Malinow. Rapid spine delivery and redistribution of ampa receptors after synaptic nmda receptor activation. *Science*, 284(5421):1811–1816, June 1999.

[47] M D'Apuzzo, G Mandolesi, G Reis, and EM Schuman. Abundant gfp expression and ltp in hippocampal acute slices by in vivo injection of sindbis virus. *Journal of Neurophysiology*, 86(2):1037–1042, August 2001.

[48] ND Lawson and BM Weinstein. In vivo imaging of embryonic vascular development using transgenic zebrafish. *Developmental Biology*, 248(2):307–318, August 2002.

[49] F Bestvater, E Spiess, G Stobrawa, M Hacker, T Feurer, T Porwol, U Berchner-Pfannschmidt, C Wotzlaw, and H Acker. Two-photon fluorescence absorption and emission spectra of dyes relevant for cell imaging. *Journal of Microscopy-Oxford*, 208:108–115, November 2002.

[50] ME Dickinson, E Simbuerger, B Zimmermann, CW Waters, and SE Fraser. Multiphoton excitation spectra in biological samples. *Journal of Biomedical Optics*, 8(3):329–338, July 2003.

[51] H. Wabnitz I. Bugiel, K. König. Investigations of cells by fluorescence laser scanning microscopy with subnanosecond resolution. *Lasers in the Life Sciences*, 3:47–53, 1989.

[52] K König, C Peuckert, I Riemann, and U Wollina. Optical tomography of human skin with subcellular resolution and picosecond time resolution using intense near infrared femtosecond laser pulses. *Proc SPIE*, (4620):191–201, 2002.

[53] Karsten Konig and Iris Riemann. High-resolution multiphoton tomography of human skin with subcellular spatial resolution and picosecond time resolution. *J Biomed Opt*, 8(3):432–9, Jul 2003.

[54] D Schweitzer, A Kolb, M Hammer, and E Thamm. Basic investigations for 2-dimensional time-resolved fluorescence measurements at the fundus. *Int Ophthalmol*, 23(4-6):399–404, 2001.

[55] Hammer M Thamm E. Schweitzer D, Kolb A. Tau-mapping of the autofluorescence of the human ocular fundus. *Proc SPIE*, (4164):79 – 89, 2000.

[56] R Sanders, A Draaijer, H C Gerritsen, P M Houpt, and Y K Levine. Quantitative ph imaging in cells using confocal fluorescence lifetime imaging microscopy. *Anal Biochem*, 227(2):302–8, May 1995.

[57] Kirby M. S. Cheng H. Lederer W. J. Piston, D. W. and W. W. Webb. Two photon excitation fluorescence imaging of three-dimensional calcium ion activity. *Appl. Optics*, (33):662–669, 1994.

[58] J R Lakowicz, H Szmacinski, K Nowaczyk, W J Lederer, M S Kirby, and M L Johnson. Fluorescence lifetime imaging of intracellular calcium in cos cells using quin-2. *Cell Calcium*, 15(1):7–27, Jan 1994.

[59] T Oida, Y Sako, and A Kusumi. Fluorescence lifetime imaging microscopy (flimscopy). methodology development and application to studies of endosome fusion in single cells. *Biophys J*, 64(3):676–85, Mar 1993.

[60] T W Gadella, Jr and T M Jovin. Oligomerization of epidermal growth factor receptors on a431 cells studied by time-resolved fluorescence imaging microscopy. a stereochemical model for tyrosine kinase receptor activation. *J Cell Biol*, 129(6):1543–58, Jun 1995.

[61] K König, P T So, W W Mantulin, B J Tromberg, and E Gratton. Two-photon excited lifetime imaging of autofluorescence in cells during uva and nir photostress. *J Microsc*, 183(Pt 3):197–204, Sep 1996.

[62] T French, P T So, D J Weaver, Jr, T Coelho-Sampaio, E Gratton, E W Voss, Jr, and J Carrero. Two-photon fluorescence lifetime imaging microscopy of macrophage-mediated antigen processing. *J Microsc*, 185(Pt 3):339–53, Mar 1997.

[63] French T. Yu W. M. Berland K. M. Dong C. Y. So, P. T. C. and E. Gratton. Time-resolved fluorescence microscopy using two-photon excitation. *Bioimaging*, (3):49–63, 1995.

[64] R. Sanders, A. Draaijer, H.C. Gerritsen, and Y.K. Levine. Selective imaging of multiple probes using fluorescence lifetime contrast. *Zoological Studies*, 34:173–174, April 1995.

[65] J A Dix and A S Verkman. Pyrene eximer mapping in cultured fibroblasts by ratio imaging and time-resolved microscopy. *Biochemistry*, 29(7):1949–53, Feb 1990.

[66] S.M. Keating and T.G. Wensel. Nanosecond fluorescence microscopy - emission kinetics of fura-2 in single cells. *Biophysical Journal*, 59(1):186–202, January 1991.

[67] E. P. Buurman, R. Sanders, A. Draaijer, H.C. Gerritsen, J.J.F. Vanveen, P.M. Houpt, and Y.K. Levine. Fluorescence lifetime imaging using a confocal laser scanning microscope. *Scanning*, 14(3):155–159, May-Jun 1992.

[68] C.G. Morgan, A.C. Mitchell, and J.G. Murray. Prospects for confocal imaging based on nanosecond fluorescence decay time. *Journal of Microscopy-Oxford*, 165:49–60, January 1992.

[69] Sandison D. R. Piston, D. W. and W. W. Webb. Time-resolved fluorescence imaging and background rejection by two-photon excitation in laser scanning microscopy. *Proc. SPIE*, (1640):379–389, 1992.

[70] C Y Dong, P T So, T French, and E Gratton. Fluorescence lifetime imaging by asynchronous pump-probe microscopy. *Biophys J*, 69(6):2234–42, Dec 1995.

[71] M. Muller, R. Ghauharali, K. Visscher, and G. Brakenhoff. Double-pulse fluorescence lifetime imaging in confocal microscopy. *Journal of Microscopy-Oxford*, 177:171–179, February 1995.

[72] W Patrick Ambrose, Peter M Goodwin, Richard A Keller, and John C Martin. Alterations of single molecule fluorescence lifetimes in near-field optical microscopy. *Science*, 265(5170):364–367, Jul 1994.

[73] X Sunney Xie and Robert C Dunn. Probing single molecule dynamics. *Science*, 265(5170):361–364, Jul 1994.

[74] Uchida T. Coleman D. M. Wang, X. F. and S. Minami. A two-dimensional fluorescence lifetime imaging system using a gated image intensifier. *Appl. Spect.*, (45):360–366, 1991.

[75] D McLoskey, DJS Birch, A Sanderson, K Suhling, E Welch, and PJ Hicks. Multiplexed single-photon counting .1. a time-correlated fluorescence lifetime camera. *Review of Scientific Instruments*, 67(6):2228–2237, June 1996.

[76] Uchida T. Wang, X. F. and S. Minami. A fluorescence lifetime distribution measurement system based on phase-resolved detection using an image dissector tube. *Appl. Spect.*, (45):840–845, 1989.

[77] G Marriott, R M Clegg, D J Arndt-Jovin, and T M Jovin. Time resolved imaging microscopy. phosphorescence and delayed fluorescence imaging. *Biophys J*, 60(6):1374–87, Dec 1991.

[78] J.R. Lakowicz and K.W. Berndt. Lifetime-selective fluorescence imaging using an rf phase-sensitive camera. *Review of Scientific Instruments*, 62(7):1727–1734, July 1991.

[79] French T. So, P. T. C. and E. Gratton. A frequency domain time-resolved microscope using a fast-scan ccd camera. *Proc. SPIE*, (2137):83–92, 1994.

[80] W. Becker, H. Stiel, and E. Klose. Flexible instrument for time-correlated single-photon counting. *Review of Scientific Instruments*, 62(12):2991–2996, December 1991.

[81] C.Y. Dong, French T., P.T.C. So, C. Buehler, K.M. Berland, and Gratton E. Fluorescence-lifetime imaging techniques for microscopy. *Methods in Cell Biology*, 72:431–464, 1998.

[82] E Gratton, S Breusegem, J Sutin, and QQ Ruan. Fluorescence lifetime imaging for the two-photon microscope: time-domain and frequency-domain methods. *Journal of Biomedical Optics*, 8(3):381–390, July 2003.

[83] F S Wouters, P J Verveer, and P I Bastiaens. Imaging biochemistry inside cells. *Trends Cell Biol*, 11(5):203–11, May 2001.

[84] Marion Peter and Simon M Ameer-Beg. Imaging molecular interactions by multiphoton flim. *Biol Cell*, 96(3):231–6, Apr 2004.

[85] Anna Peyker, Oliver Rocks, and Philippe I H Bastiaens. Imaging activation of two ras isoforms simultaneously in a single cell. *Chembiochem*, 6(1):78–85, Jan 2005.

[86] Marion Peter, Simon M Ameer-Beg, Michael K Y Hughes, Melanie D Keppler, Søren Prag, Mark Marsh, Borivoj Vojnovic, and Tony Ng. Multiphoton-flim quantification of the egfp-mrfp1 fret pair for localization of membrane receptor-kinase interactions. *Biophys J*, 88(2):1224–37, Feb 2005.

[87] K Suhling, J Siegel, D Phillips, P M French, S Lévêque-Fort, S E Webb, and D M Davis. Imaging the environment of green fluorescent protein. *Biophys J*, 83(6):3589–3595, Dec 2002.

[88] P J Verveer, A Squire, and P I Bastiaens. Global analysis of fluorescence lifetime imaging microscopy data. *Biophys J*, 78(4):2127–37, Apr 2000.

[89] S Pelet, M J R Previte, L H Laiho, and P T C So. A fast global fitting algorithm for fluorescence lifetime imaging microscopy based on image segmentation. *Biophys J*, 87(4):2807–17, Oct 2004.

[90] A H A Clayton, Q S Hanley, and P J Verveer. Graphical representation and multicomponent analysis of single-frequency fluorescence lifetime imaging microscopy data. *J Microsc*, 213(Pt 1):1–5, Jan 2004.

[91] Glen I Redford and Robert M Clegg. Polar plot representation for frequency-domain analysis of fluorescence lifetimes. *J Fluoresc*, 15(5):805–15, Sep 2005.

[92] Ryan A. Colyer, Claudia Lee, and Enrico Gratton. A novel fluorescence lifetime imaging system that optimizes photon efficiency. *Microscopy Research and Technique*, 71(3):201–213, March 2008.

[93] ST Hess, ED Sheets, A Wagenknecht-Wiesner, and AA Heikal. Quantitative analysis of the fluorescence properties of intrinsically fluorescent proteins in living cells. *Biophysical Journal*, 85(4):2566–2580, October 2003.

[94] P Bornstein, A H Kang, and K A Piez. The nature and location of intramolecular cross-links in collagen. *Proc Natl Acad Sci U S A*, 55(2):417–24, Feb 1966.

[95] S. L. Bel'Kov, M. V. B. Fluorescence spectra and kinetics of isomers and dimers of retinoic acid. *Journal of Applied Spectroscopy*, 53(6):1271âĂŘ1275, 1990.

[96] Thomas H. Chia, Anne Williamson, Dennis D. Spencer, and Michael J. Levene. Multiphoton fluorescence lifetime imaging of intrinsic fluorescence in human and rat brain tissue reveals spatially distinct nadh binding. *Optics Express*, 16(6):4237–4249, March 2008.

[97] J R Lakowicz, H Szmacinski, K Nowaczyk, and M L Johnson. Fluorescence lifetime imaging of free and protein-bound nadh. *Proc Natl Acad Sci U S A*, 89(4):1271–5, Feb 1992.

[98] Lorenzo Brancaleon, Steven W Magennis, Ifor D W Samuel, Ebinazar Namdas, Andrea Lesar, and Harry Moseley. Characterization of the photoproducts of protoporphyrin ix bound to human serum albumin and immunoglobulin g. *Biophys Chem*, 109(3):351–60, Jun 2004.

[99] Irina Eberle, Birgit Pless, Miriam Braun, Theo Dingermann, and Rolf Marschalek. Transcriptional properties of human nanog1 and nanog2 in acute leukemic cells. *Nucleic Acids Res*, Apr 2010.

[100] J. L. Baran, A. C. Laga, L. M. Duncan, and G. F. Murphy. The embryonic stem cell transcription factor sox2 is expressed by spitz nevi. In *Laboratory Investigation*, volume 90, pages 111A–111A, 75 VARICK ST, 9TH FLR, NEW YORK, NY 10013-1917 USA, February 2010. NATURE PUBLISHING GROUP.

[101] Ian Chambers and Simon R. Tomlinson. The transcriptional foundation of pluripotency. *Development*, 136(14):2311–2322, July 2009.

[102] Candace L. Kerr, Christine M. Hill, Paul D. Blumenthal, and John D. Gearhart. Expression of pluripotent stem cell markers in the human fetal testis. *Stem Cells*, 26(2):412–421, February 2008.

[103] J Nichols, B Zevnik, K Anastassiadis, H Niwa, D Klewe-Nebenius, I Chambers, H Scholer, and A Smith. Formation of pluripotent stem cells in the mammalian embryo depends on the pou transcription factor oct4. *Cell*, 95(3):379–391, October 1998.

[104] Jimmy Susanto, Yu-Hsing Lin, Yun-Nan Chen, Chia-Rui Shen, Yu-Ting Yan, Sheng-Ta Tsai, Chung-Hsuan Chen, and Chia-Ning Shen. Porphyrin homeostasis maintained by abcg2 regulates self-renewal of embryonic stem cells. *PLoS One*, 3(12):e4023, 2008.